CrossMark

A Thermo-Magneto-Mechanically Coupled Constitutive Model of Magnetic Shape Memory Alloys

Chao Yu[1,2]   Guozheng Kang[1,2]*   Daining Fang[3]

([1]*State Key Laboratory of Traction Power, Southwest Jiaotong University, Chengdu 610031, China*)
([2]*Applied Mechanics and Structure Safety Key Laboratory of Sichuan Province, School of Mechanics and Engineering, Southwest Jiaotong University, Chengdu 610031, China*)
([3]*Institute of Advanced Technology, Beijing Institute of Technology, Beijing 100081, China*)

ABSTRACT A macroscopic phenomenological constitutive model considering the martensite transformation and its reverse is constructed in this work to describe the thermo-magneto-mechanically coupled deformation of polycrystalline magnetic shape memory alloys (MSMAs) by referring to the existing experimental results. The proposed model is established in the framework of thermodynamics by introducing internal state variables. The driving force of martensite transformation, the internal heat production and the thermodynamic constraints on constitutive equations are obtained by Clausius dissipative inequality and constructed Gibbs free energy. The spatiotemporal evolution equation of temperature is deduced from the first law of thermodynamics. The demagnetization effect occurring in the process of magnetization is also addressed. The proposed model is verified by comparing the predictions with the corresponding experiments. It is concluded that the thermo-magneto-mechanically coupled deformation of MSMAs including the magnetostrictive and magnetocaloric effects at various temperatures can be reasonably described by the proposed model, and the magnetocaloric effect can be significantly improved over a wide range of temperature by introducing an additional applied stress.

1. Introduction

Magnetic shape memory alloys (MSMAs) are a new kind of smart materials and have attracted increasing interest due to their large recoverable magnetic field-induced strain (MFIS). Besides the well-known shape memory effect and super-elasticity observed in conventional shape memory alloys (SMAs), MSMAs can work in a very high frequency up to an order of kHz, because their martensite transformation and/or reorientation can also be driven by the magnetic field. Recently, MSMAs have been successfully used in many engineering fields, for instance, actuator and sensor applications, solid-state refrigeration, biomedical engineering [1–4].

There are two possible mechanisms to obtain a large reversible strain in MSMAs: one is the reorientation of martensite variants as a result of twin boundary motion; the other is the transformation

---

*   Corresponding author. E-mail: guozhengkang@home.swjtu.edu.cn; guozhengkang@126.com

occurring between the austenite and martensite phases. Since different martensite variants have different eigenstrains and preferred magnetization directions, an applied stress or magnetic field can be used to activate the production of certain variants from the others through the movement of twin boundary, which is called the magnetic field-induced martensite reorientation (MFIR), resulting in a macroscopic strain as reported in NiMnGa [5–10] and further in other MSMAs such as FePd [11], NiMnAl [12], FePt [13], NiCoGa [14] and NiCoAl [15]. As discussed by Karaca et al. [16], two key requirements for the occurrence of MFIR are low twinning stress and high magnetocrystalline anisotropy energy. The low twinning stress leads to a low actuation stress (only several MPa s) in the actuator made by MSMAs, while the high magnetocrystalline anisotropy energy makes the MFIR occur only in the MSMA single crystals or the polycrystalline aggregates with very strong initial textures [17–19].

The second mechanism can also be denoted as the magnetic field-induced transformation (MFIT). Since the differences of the eigenstrain and entropy between the austenite and martensite phases are significant in MSMAs, the martensite transformation can also be induced by the applied stress and/or temperature. However, the driving force of MFIT is the difference of Zeeman energies between the austenite and martensite phases. Thus, an effective approach to promote the occurrence of magnetic field-induced martensite transformation is to enhance the magnetization difference between the two phases. Sutou et al. [20] and Kainuma et al. [21] reported that in NiMnIn, NiMnSb and NiMnSn single crystals, the compressive pre-strain caused by the stress-induced martensite transformation could be fully recovered when a magnetic field was applied in parallel to the compressive axis of specimen. Such phenomenon was explained as the magnetic field-induced reverse transformation (i.e., from the martensite to austenite phase). From a view point of energy, the reverse transformation can reduce the total Zeeman energy when a magnetic field is applied, since the magnetization of martensite phase is much lower than that of austenite phase in the alloys. Thus, the reverse transformation will be triggered when the magnetic field reaches a critical value. Comparing to the MFIR, the MFIT can provide high actuation stress and work output. Kainuma et al. [21] predicted that the actuation stress caused by MFIT in NiMnCoIn should be the order of tens of MPas according to the Clausius–Clapeyron relation. The high actuation stress and work output of NiMnCoIn MSMA single crystal were systematically and experimentally investigated by Karaca [16]. It was found that the single crystal with an orientation of [111] demonstrated a very high magnetostress (e.g., 140 MPa/T), but the work output is almost independent of the crystallographic orientation. Although the actuation stress has been significantly improved by the mechanism of MFIT, the high cost of single crystal restricts the wide application of MSMAs. Fortunately, unlike the magnetocrystalline anisotropy energy, the Zeeman energy does not strongly depend on the crystallographic orientation. So, the mechanism of MFIT can also be triggered in the polycrystalline aggregates without strong initial textures, as reported by [22].

The thermal effects caused by the applied stress and magnetic fields in the materials are called the elastocaloric and magnetocaloric effects, respectively. Since the stress/magnetic field-induced martensite transformation is accompanied by the release/absorption of a large amount of latent heat, another important application of MSMAs is found in the solid-state refrigeration [4, 23–28]. Recently, many polycrystalline MSMAs, e.g., NiMnIn, NiMnInCo, NiMnCoSn and CoNiAl, are considered as very promising candidates for the solid-state refrigerators due to their partially reversible magnetocaloric effect during the repeated application and removal of magnetic field, excellent mechanical stability and low cost.

To reasonably design the actuators, sensors and refrigerators made from MSMAs, a constitutive model is urgently necessary. In the last two decades, many constitutive models have been constructed. For example, by introducing the chemical, mechanical, magnetic and thermal energies, Hirsinger and Lexcellent [29, 30] established a 2D constitutive model of NiMnGa MSMAs based on irreversible thermodynamics, which could be simply denoted as the H-L model. In the H-L model, two types of internal variables, i.e., the volume fractions of martensite variants and magnetic domains, were introduced to characterize the microstructures of the alloy, and the magnetization vector in each variant was assumed to be always aligned with the magnetic easy axis and not rotate away in the process of magnetization. Kiefer and Lagoudas [31] extended the H-L model [29, 30] by considering three mechanisms, i.e., martensite reorientation, magnetic domain wall motion and magnetization vector rotation, simultaneously. Wang and Li [32] proposed a kinetic model by introducing a tensorial description of kinetics and

developed an explicit kinetic evolution formulation to describe the martensite reorientation under magnetic and mechanical loading. Couch and Chopra [33] proposed a simplified phenomenological model for NiMnGa MSMAs, where the stress was assumed to be a linear combination of strains, volume fractions of martensite variants and magnetic field. Zhu and Dui [34–36] constructed a micromechanical constitutive model based on the Eshelby's equivalent inclusion method and Mori-Tanaka homogenization scheme. Wang et al. [37] extended the model proposed by Zhu and Dui [34–36] and studied the influence of material anisotropy and inclusion morphology on the reorientation. By introducing three martensite variants and considering the compatibility of constitutive equations with thermodynamics, Chen et al. [38], Auricchio et al. [39] and Mousavi and Arghavani [40] proposed some 3D constitutive models, which well described the strain magnetization responses of MSMAs under arbitrary complex magneto-mechanical loading conditions. Pei and Fang [41] proposed a simple model by extending the transformation kinetics of conventional SMAs and introduced the magnetic field-induced stress and an equivalence principle to describe the mechanical and magnetoelastic deformation. LaMaster et al. [42, 43] proposed 2D and 3D constitutive models of MSMAs by addressing the demagnetization effect during the magnetization. It should be noted that the constitutive models mentioned above focus on the stress and magnetic field-induced martensite reorientation in MSMA single crystals only. Recently, a thermodynamics-based constitutive model considering the MFIT of NiMnCoIn MSMA single crystals was proposed by Haldar et al. [44]. The elastic and magnetic properties of austenite and martensite phases were analyzed by the group theory in [44], and then the influences of temperature and stress on the MFIS could be reasonably predicted.

Although the constitutive models of MSMAs have been greatly developed, most of them only focus on the stress and magnetic field-induced martensite reorientation in single crystals. Thus, they are not suitable to describe the martensite transformation of polycrystalline MSMAs occurring under the multi-field-coupled loading conditions (e.g., the coupling of stress, temperature and magnetic fields). Moreover, since the internal heat produced during the deformation and magnetization was not considered, the existing models [29–44] could not reasonably describe the elastocaloric and magnetocaloric effects existed in MSMAs.

The aim of this work is to construct a macroscopic phenomenological constitutive model to describe the thermo-magneto-mechanically coupled deformation of polycrystalline MSMAs and provide a theoretical guidance for the design of device made by MSMAs. The proposed model focuses on the multi-field-induced martensite transformation and the internal heat production during the deformation and magnetization, and is established in a framework of thermodynamics. The demagnetization effect is also addressed in the proposed model. The comparison between the simulated results and the experimental ones shows that the thermo-magneto-mechanically coupled deformation of polycrystalline MSMAs, including the magnetostrictive and magnetocaloric effects at various temperatures, can be reasonably described by the proposed model. Also, the influence of applied stress on the magnetocaloric effect is discussed.

2. Outline of Experimental Phenomena

To keep the integrity of the content, in this section, typical experimental phenomena for the magnetostrictive and magnetocaloric effects of polycrystalline MSMAs obtained by Lázpita et al. [45] and Liu et al. [23] are outlined. The details can be referred to the original literature.

2.1. Magnetostrictive Effect of MnNiFeSn MSMA

In the experiments of Lázpita et al. [45], the materials were polycrystalline $Mn_{49}Ni_{42-x}Fe_xSn_9$ alloys with $x = 0, 2, 3, 4, 5$ and 6 (where x is the atom percentage). The geometric dimension of the sample is 3.0 mm × 2.0 mm × 1.5 mm. The effect of Fe doping on the magnetic field- and temperature-induced martensite transformations of MnNiFeSn MSMAs was systematically investigated. It was found that when $x = 4$, the alloy could present the largest magnetostrictive strain. Therefore, the experimental results of $Mn_{49}Ni_{38}Fe_4Sn_9$ MSMA ($x = 4$) are outlined here and will be simulated by the proposed model in this work. In the absence of magnetic field, the finish temperature of austenite (A_f^0), start temperature of austenite (A_s^0), start temperature of martensite (M_s^0) and finish temperature of martensite (M_f^0) of $Mn_{49}Ni_{38}Fe_4Sn_9$ MSMA were detected as 230 K, 206 K, 221.5 K and 195.5 K,
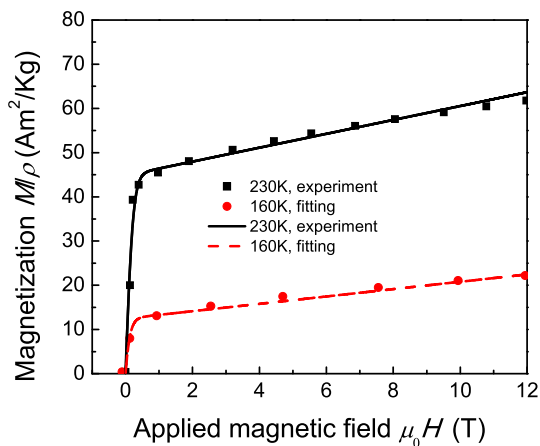
Fig. 1. Curves of applied magnetic field versus magnetization for MnNiFeSn MSMA at 160 K and 230 K (the experimental results are cited from Lázpita et al. [45])

respectively. The superscript "0" represents that the critical temperatures are under zero magnetic field.

Figure 1 shows the curves of applied magnetic field versus magnetization for the $Mn_{49}Ni_{38}Fe_4Sn_9$ MSMA at various temperatures, i.e., 160 K (at which the alloy consists of the martensite phase) and 230 K (at which the alloy consists of the austenite phase), respectively. The loading rate of magnetic field is very small and can be regarded as the isothermal case. From Fig. 1, it is seen that once a magnetic field is applied, the magnetization of austenite and martensite phases increases rapidly, but is not fully saturated even at 12 T. Under a given magnetic field, the magnetization of austenite phase is much larger than that of martensite one.

Figure 2a–e shows the curves of temperature versus strain obtained for the $Mn_{49}Ni_{38}Fe_4Sn_9$ MSMA during a cooling–heating cycle (that is, the specimen is cooled to 150 K and then heated to the test temperature) under the applied magnetic fields of 0 T, 1 T, 3 T, 7 T and 12 T, respectively. From Fig. 2a, it is seen that at the beginning of cooling (segment o-a), a linear reduction of the length is observed, which is caused by the thermal expansion. When the temperature decreases to a critical value (point a), martensite transformation occurs, accompanied by a large amount of inelastic strain (about 0.4%). The inelastic strain is originated from the volume difference between the austenite and martensite phases, as discussed by Lázpita et al. [45]. After the martensite transformation is completed (point b), only the thermal expansion can be observed in the subsequent cooling process (segments b–c). During the heating, the reverse transformation (from the martensite to austenite phase) starts and completes at points d and e, respectively. The curves of temperature versus strain present a large hysteresis loop since the martensite transformation is a typical first-order transformation. Comparing Fig. 2b–e with Fig. 2a, it is seen that four critical temperatures shift down with the increase of applied magnetic field, which implies that the magnetic field can stabilize the austenite phase and enhance the transformation resistance.

Figure 3 shows the temperature magnetization response during a cooling–heating cycle under an applied magnetic field of 9 T. It is seen that there is a large drop of magnetization in the process of martensite transformation, which is related to the weak magnetism of martensite phase. Moreover, the magnetizations of austenite and martensite phases depend strongly on the temperature.

Figure 4a, b shows the curves of magnetic field versus strain (magnetostrictive effect) for the Mn49Ni38Fe4Sn9 MSMA at various temperatures (e.g., 150 K, 200 K, 210 K, 220 K, 250 K and 310 K). Each sample was initially cooled to 150 K and then heated to the prescribed temperatures. It is seen that at the temperature far from A_s, the magnetostrictive strain almost keeps as zero even if the applied magnetic field is increased to 12 T. At the temperature close to A_s, a nonlinear magnetic field strain hysteretic behavior occurs, and a large strain is produced during the loading of magnetic field and fully recovered after the unloading of magnetic field. In fact, when the temperature is close to A_s, the reverse transformation (from the martensite to austenite phase) can be induced by the magnetic
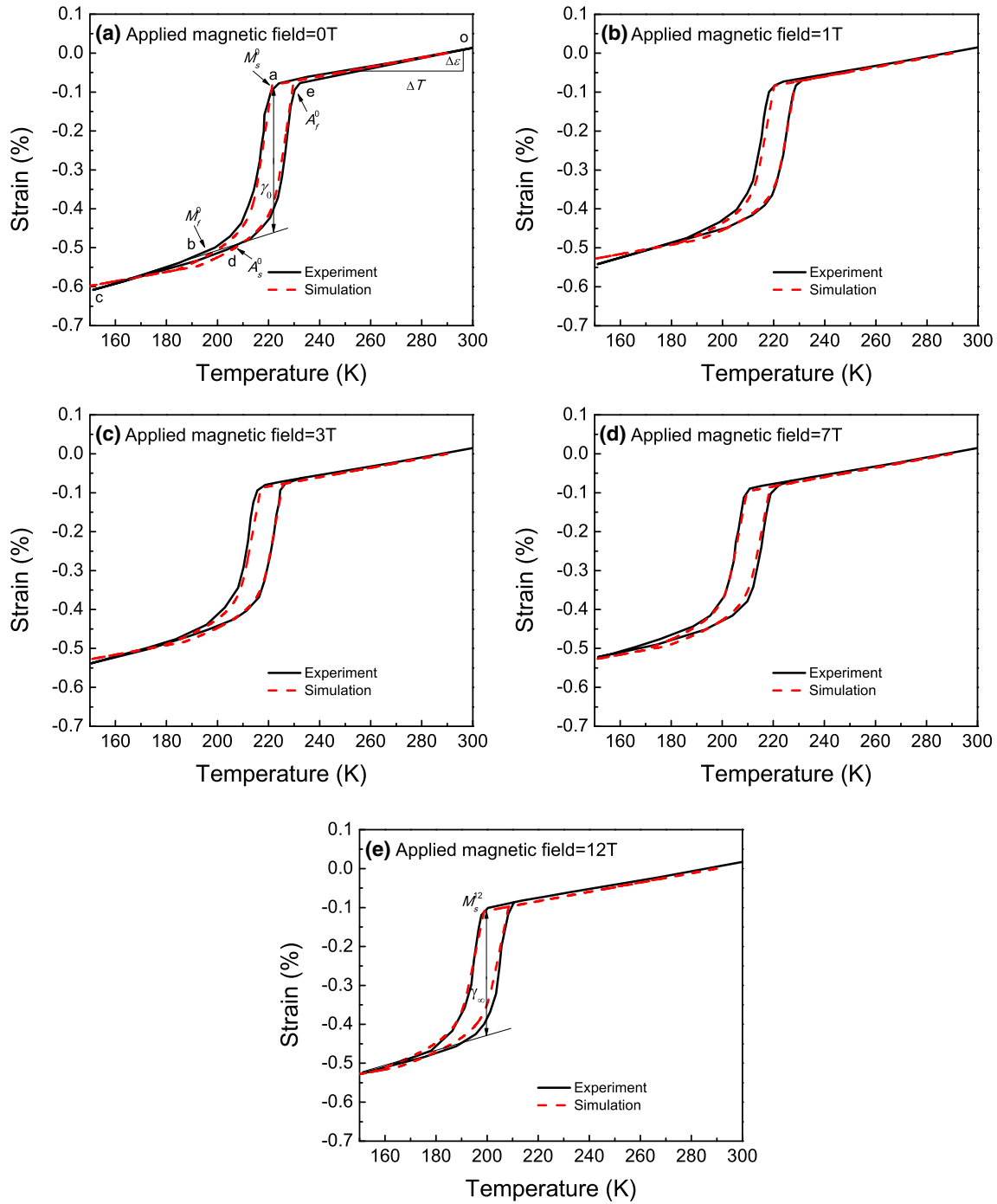
Fig. 2. Temperature-induced martensite transformation of MnNiFeSn MSMA under different magnetic fields: **a** 0 T; **b** 1 T; **c** 3 T; **d** 7 T; **e** 12 T (the experimental results are cited from Lázpita et al. [45])

field since the Zeeman energy of austenite phase is much lower than that of martensite phase. Then, a large transformation strain occurs, as shown in Fig. 4a, b.

2.2. Magnetocaloric Effect of NiMnInCo MSMA

In the experiments of Liu et al. [23], the materials were polycrystalline $Ni_{45.2}Mn_{36.7}In_{13}Co_{5.1}$, $Ni_{49.8}Mn_{35}In_{15.2}$ and $Ni_{50.4}Mn_{34.8}In_{15.8}$ MSMAs. The geometric dimension of the sample was
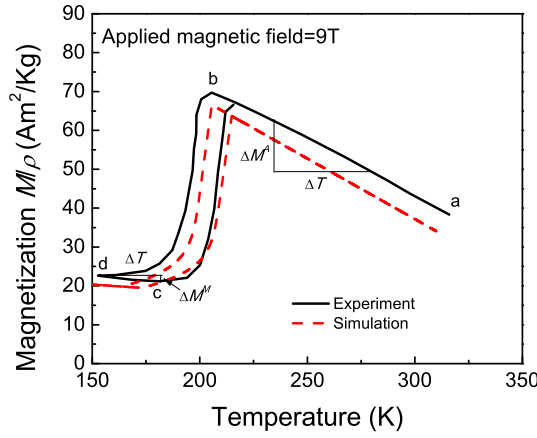
Fig. 3. Temperature magnetization response of MnNiFeSn MSMA under an applied magnetic field of 9 T (the experimental results are cited from Lázpita et al. [45])
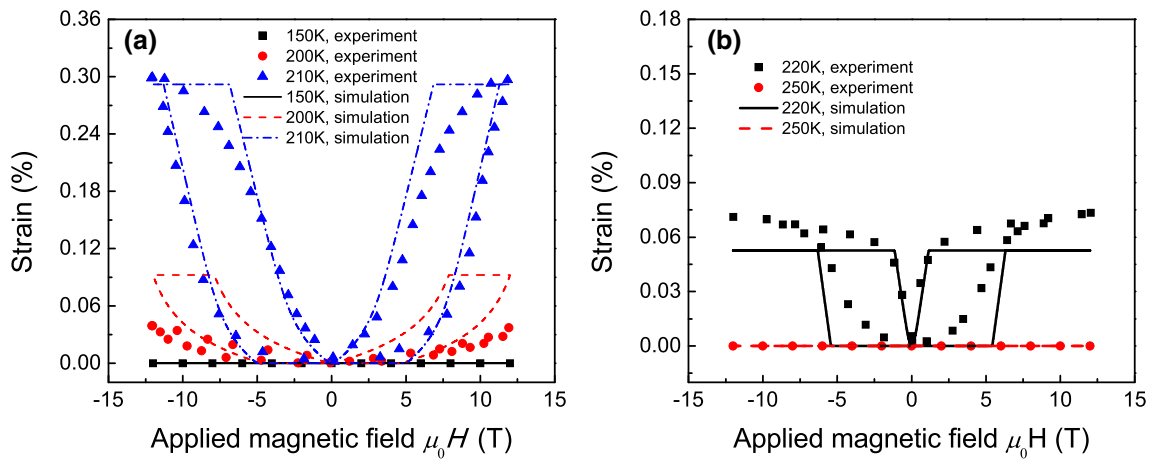

Fig. 4. Magnetic field-induced martensite transformation (magnetostrictive effect) of MnNiFeSn MSMA under an applied magnetic field of 9 T (the experimental results are cited from Lázpita et al. [45])

4.0 mm × 2.0 mm × 1.0 mm. Experimental results showed that the $Ni_{45.2}Mn_{36.7}In_{13}Co_{5.1}$ MSMA could exhibit the most remarkable magnetocaloric effect. Therefore, the experimental results of $Ni_{45.2}Mn_{36.7}In_{13}Co_{5.1}$ MSMA are outlined here and will be simulated by the model proposed in this work. Under a very small magnetic field (e.g., 0.01 T), four critical temperatures of $Ni_{45.2}Mn_{36.7}In_{13}Co_{5.1}$ MSMA, i.e., $A_f^{0.01}$, $A_s^{0.01}$, $M_s^{0.01}$ and $M_f^{0.01}$, were measured as 327 K, 317 K, 319 K and 311 K, respectively. The superscript "0.01" represents that the critical temperatures are obtained under an applied magnetic field of 0.01 T.

Figure 5 shows the temperature magnetization response of $Ni_{45.2}Mn_{36.7}In_{13}Co_{5.1}$ MSMA obtained during a quasi-static cooling–heating cycle under an applied magnetic field of 2 T. Four critical temperatures are denoted as A_f^2, A_s^2, M_s^2 and M_f^2, respectively. It is seen that the austenite and martensite phases exhibit ferromagnetism and nonmagnetism, respectively. Comparing to $A_f^{0.01}$, $A_s^{0.01}$, $M_s^{0.01}$ and $M_f^{0.01}$, four critical temperatures under an applied magnetic field of 2 T (i.e., A_f^2, A_s^2, M_s^2 and M_f^2) shift down, which means that the magnetic field can hinder the forward martensite transformation but promote the reverse one.

Figure 6 shows the temperature changes obtained under an applied magnetic field of 2 T and at various temperatures (i.e., the magnetocaloric effect). Since the loading rate of magnetic field is very high, the magnetocaloric effect can be regarded as an adiabatic process. In Liu et al. study [23], to avoid the influence of thermal history on the magnetocaloric effect, each sample was initially heated above a
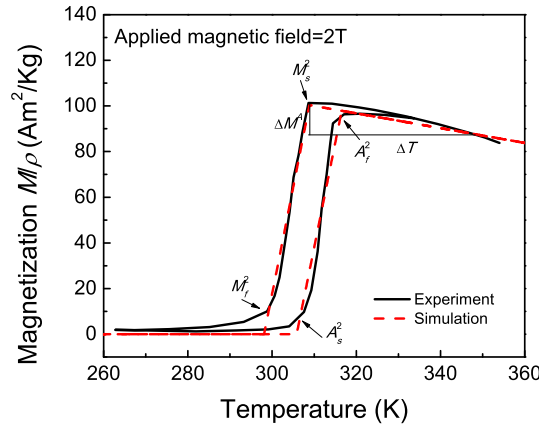
Fig. 5. Temperature magnetization response of NiMnInCo MSMA under an applied magnetic field of 2 T (the experimental results are cited from Liu et al. [23])
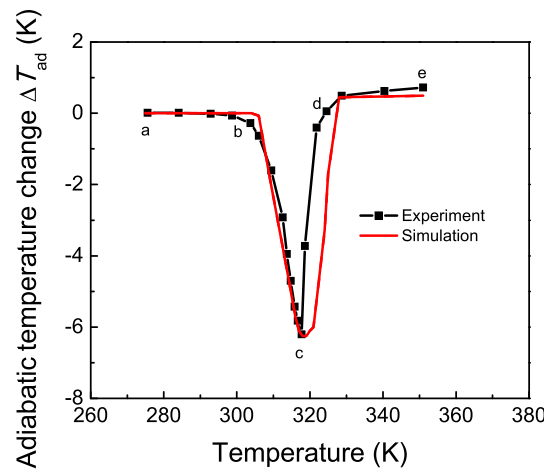

Fig. 6. Adiabatic temperature changes under an applied magnetic field of 2 T at various temperatures (magnetocaloric effect) (the experimental results are cited from Liu et al. [23])

fully austenitic state and then cooled down to a completely martensitic state. Afterward, the sample was heated to the prescribed temperature. Then, a magnetic field was applied under adiabatic conditions. From Fig. 6, it is seen that the MSMA exhibits a good refrigerating capacity, i.e., the maximum temperature change (about -6.2 K) occurs at 317 K, which is mainly caused by the absorption of transformation latent heat during the magnetic field-induced reverse transformation. However, the refrigerating capacity decreases rapidly when the test temperature deviates a little bit from 317 K. In other words, such an alloy can only be used within a very narrow temperature range.

Figure 7 shows the evolution of temperature change at 317 K during a cyclic loading of magnetic field, i.e., first loading (0 T $\rightarrow$ 2 T), unloading (2 T $\rightarrow$ 0 T), reverse loading (0 T $\rightarrow$ $-$ 2 T) and reverse unloading ($-$ 2 T $\rightarrow$ 0 T). It is seen that the first loading of magnetic field up to 2 T causes a cooling effect of $-$ 6.2 K. During the unloading of magnetic field, the sample heats only by 1.3 K and the temperature cannot fully recover to its initial value. After the sample is reversely loaded up to a magnetic field of $-$ 2 T and then unloaded to 0 T, a small temperature change of 1.3 K is obtained. It means that in the cycle refrigeration, only a temperature change of 1.3 K can be achieved in each cycle. As discussed by Liu et al. [23], the unrecoverable temperature change is originated from the large hysteresis loops of applied magnetic field and magnetization in NiMnInCo MSMA, i.e., the austenite phase cannot fully transform into the martensite one even if the applied magnetic field is
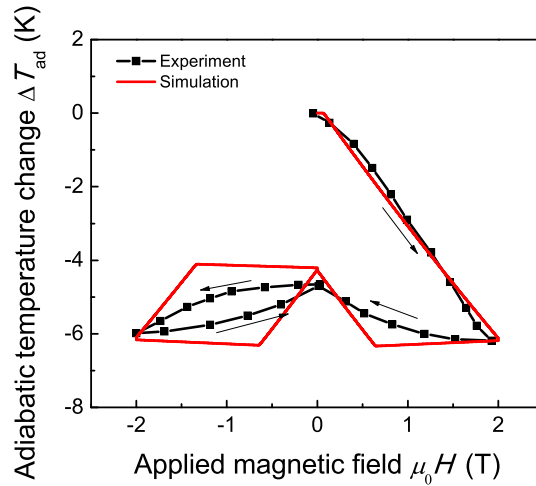
Fig. 7. Evolution of adiabatic temperature change at 317 K during a cyclic loading of magnetic field, i.e., first loading ($0\,\mathrm{T} \to 2\,\mathrm{T}$), unloading ($2\,\mathrm{T} \to 0\,\mathrm{T}$), reverse loading ($0\,\mathrm{T} \to -\,2\,\mathrm{T}$) and reverse unloading ($-\,2\mathrm{T} \to 0\,\mathrm{T}$) (the experimental results are cited from Liu et al. [23])

unloaded. Therefore, to improve the refrigerating efficiency of MSMAs, an effective way is to reduce their hysteresis loops of applied magnetic field and magnetization.

The magnetocaloric effect of MSMAs is a typical thermo-magnetically coupled process. On the one hand, during a loading of magnetic field, transformation latent heat, intrinsic dissipation, thermoelastic deformation and magnetization will lead to an internal heat production and then cause a temperature variation. On the other hand, the experimental results shown in Figs. 3 and 5 demonstrate that the martensite transformation and magnetization depend strongly on the temperature. The internal heat production and temperature-dependent material deformation influence each other, which leads to a complex thermo-magnetic response of MSMAs. Recently, the experimental results [46, 47] showed that the hysteresis loops of applied magnetic field and magnetization in MSMAs could be manipulated by applying an additional stress (such as hydrostatic pressure), which suggested a candidate to improve the refrigerating efficiency of MSMAs. So, a thermo-magnetic-mechanically coupled problem must be faced up in this aspect.

As commented in Sect. 1, the existing constitutive models addressed the magneto-mechanically coupled deformation of MSMA single crystals only, and did not describe the experimental results outlined in this section reasonably. Thus, a macroscopic thermo-magneto-mechanically coupled constitutive model is necessary to describe the outlined experimental observations here, which will be constructed in Sect. 3.

3. Constitutive Model

3.1. Inelastic Strain and Magnetization Vector

The proposed model is constructed based on the hypothesis of small deformation, since the maximum transformation strain of MSMAs does not exceed 10%. Considering the contributions of elastic deformation, thermal expansion and martensite transformation, the total strain tensor $\boldsymbol{\varepsilon}$ is decomposed into three parts, i.e.,

$$\boldsymbol{\varepsilon} = \boldsymbol{\varepsilon}^{\mathrm{e}} + \boldsymbol{\varepsilon}^{\mathrm{T}} + \boldsymbol{\varepsilon}^{\mathrm{tr}} \qquad (1)$$

where $\boldsymbol{\varepsilon}^{\mathrm{e}}$, $\boldsymbol{\varepsilon}^{\mathrm{T}}$ and $\boldsymbol{\varepsilon}^{\mathrm{tr}}$ are the elastic, thermal expansion and transformation strain tensors, respectively.

The relationship between the thermal expansion strain $\boldsymbol{\varepsilon}^{\mathrm{T}}$ and temperature T is written as:

$$\boldsymbol{\varepsilon}^{\mathrm{T}} = \boldsymbol{\alpha}\,(T - T_0) \qquad (2)$$

where $\boldsymbol{\alpha}$ is the second-order thermal expansion tensor, T is temperature, and T_0 is the balance temperature. In this work, $\boldsymbol{\alpha}$ is regarded as an isotropic tensor for simplicity, i.e., $\boldsymbol{\alpha} = \alpha\mathbf{1}$, where $\mathbf{1}$ is the second-order unit tensor.
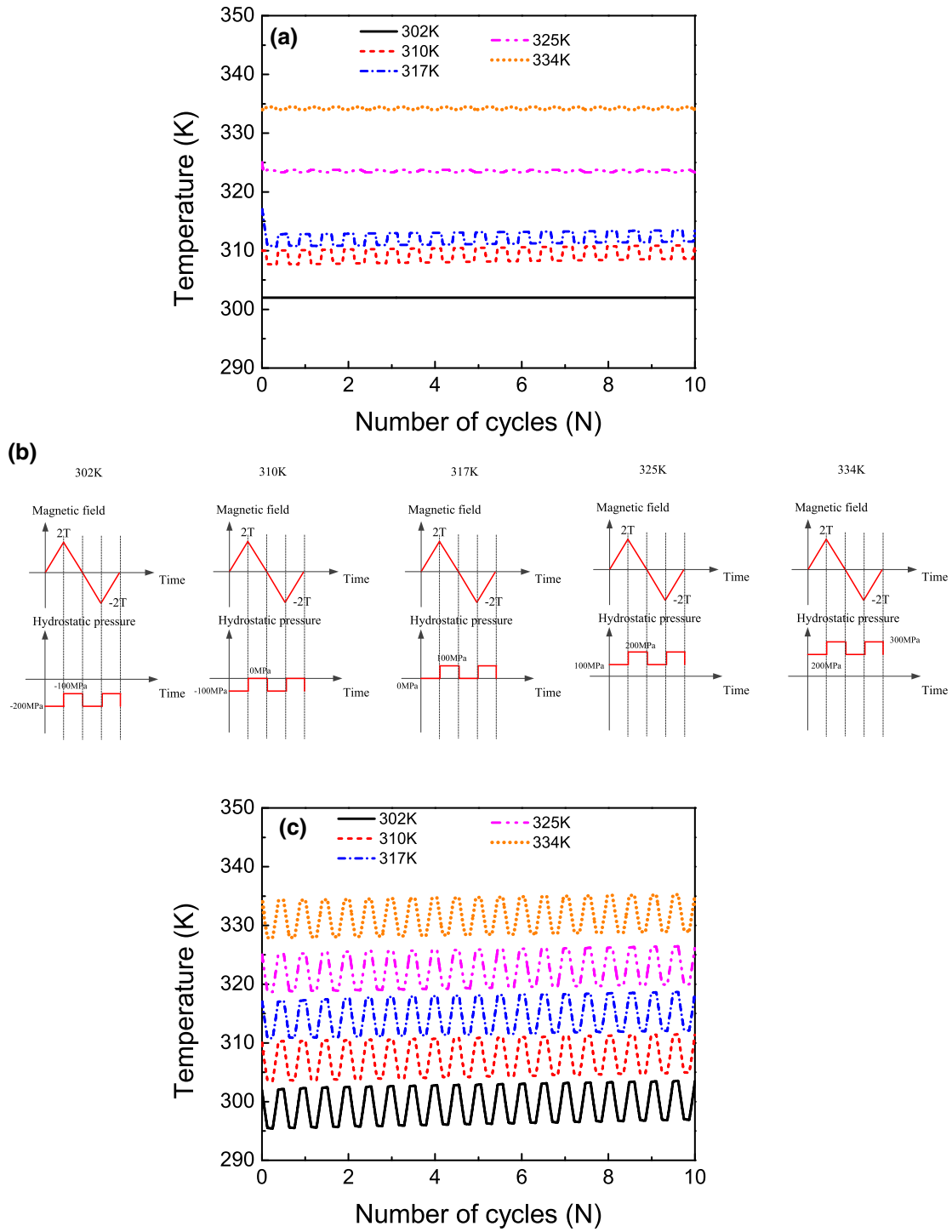
Fig. 8. Evolution of adiabatic temperature change under the cyclic loading of magnetic field (with 10 cycles) at various ambient temperatures: **a** predicted results without stress manipulation; **b** magneto-mechanically coupled loading paths in each cycle at various temperatures; **c** predicted results with stress manipulation

It is assumed that there is a linear relationship between the rates of transformation strain $\dot{\boldsymbol{\varepsilon}}^{\text{tr}}$ and martensite volume fraction $\dot{\xi}$, i.e.,

$$\dot{\boldsymbol{\varepsilon}}^{\text{tr}} = \dot{\xi} \boldsymbol{\Lambda}^{\text{tr}} \tag{3}$$

where $\boldsymbol{\Lambda}^{\mathrm{tr}}$ is the direction tensor of martensite transformation. Referring to Qidwai [48] and Lagoudas et al. [49], $\boldsymbol{\Lambda}^{\mathrm{tr}}$ can be written as:

$$\boldsymbol{\Lambda}^{\mathrm{tr}} = \begin{cases} \sqrt{\dfrac{3}{2}} H^{\mathrm{max}}\left(\boldsymbol{\sigma}, T, \boldsymbol{H}\right) \dfrac{\mathrm{dev}(\boldsymbol{\sigma})}{\|\mathrm{dev}(\boldsymbol{\sigma})\|} + \gamma\left(\boldsymbol{\sigma}, T, \boldsymbol{H}\right) \mathbf{1} & \text{when } \dot{\xi} > 0 \\ \dfrac{\varepsilon_{\mathrm{r}}^{\mathrm{tr}}}{\xi_{\mathrm{r}}} & \text{when } \dot{\xi} < 0 \end{cases} \tag{4}$$

where H^{max} is the maximum shear strain, and γ is the volumetric strain caused by martensite transformation, and they are generally the functions of stress $\boldsymbol{\sigma}$, temperature T and internal magnetic field $\boldsymbol{H}$. It should be noted that in the conventional SMAs such as the NiTi alloys, the volumetric change during the martensite transformation is very small and is often neglected [50, 51]. However, in many MSMAs, the volumetric strain caused by the martensite transformation can be about 1% [45, 52] and should be considered in the constitutive model. $\mathrm{dev}\left(\boldsymbol{\sigma}\right)$ is the deviatoric stress tensor. $\boldsymbol{\varepsilon}_{\mathrm{r}}^{\mathrm{tr}}$ and ξ_{r} are the transformation strain and the volume fraction of martensite at the beginning of reverse transformation, respectively.

For MSMAs, under a magnetic field, the magnetization vectors in austenite and martensite phases tend to be aligned with the external magnetic field by two magnetization mechanisms, i.e., the motion of magnetic domain wall and the rotation of magnetization vector. Here, the microscopic magnetization mechanisms are not considered, since the proposed model is a macroscopic phenomenological one. Owing to the random orientations of grains, the magnetization property of polycrystalline MSMAs can be regarded as isotropic. Therefore, the direction of the magnetization vectors in austenite and martensite phases ($\boldsymbol{M}^{\mathrm{A}}$ and $\boldsymbol{M}^{\mathrm{M}}$) is assumed to be aligned with the external magnetic field, respectively, i.e.,

$$\boldsymbol{M}^{\mathrm{A}} = f\left(\boldsymbol{H}, T, \boldsymbol{\sigma}\right) \frac{\boldsymbol{H}}{|\boldsymbol{H}|} \tag{5a}$$

$$\boldsymbol{M}^{\mathrm{M}} = g\left(\boldsymbol{H}, T, \boldsymbol{\sigma}\right) \frac{\boldsymbol{H}}{|\boldsymbol{H}|} \tag{5b}$$

where $f\left(\boldsymbol{H}, T, \boldsymbol{\sigma}\right)$ and $g\left(\boldsymbol{H}, T, \boldsymbol{\sigma}\right)$ are the magnetization intensities of austenite and martensite phases, respectively. Generally, they are the functions of stress $\boldsymbol{\sigma}$, temperature T and internal magnetic field $\boldsymbol{H}$.

Adopting the mixture rule, the total magnetization vector of a material point can be written as:

$$\boldsymbol{M} = (1 - \xi)\boldsymbol{M}^{\mathrm{A}} + \xi\boldsymbol{M}^{\mathrm{M}} = F\left(\boldsymbol{H}, T, \boldsymbol{\sigma}, \xi\right) \frac{\boldsymbol{H}}{|\boldsymbol{H}|} \tag{6}$$

where $F\left(\boldsymbol{H}, T, \boldsymbol{\sigma}, \xi\right) = (1 - \xi) f\left(\boldsymbol{H}, T, \boldsymbol{\sigma}\right) + \xi g\left(\boldsymbol{H}, T, \boldsymbol{\sigma}\right)$.

The magnetic field caused by the body's own magnetization is called the demagnetizing field. If a uniform external magnetic field $\boldsymbol{H}^{\mathrm{app}}$ is applied, the internal magnetic field of a material point $\boldsymbol{x}$ can be written as:

$$\boldsymbol{H}\left(\boldsymbol{x}\right) = \boldsymbol{H}^{\mathrm{app}} + \boldsymbol{H}^{\mathrm{d}}\left(\boldsymbol{x}\right) \tag{7}$$

where $\boldsymbol{H}^{\mathrm{d}}\left(\boldsymbol{x}\right)$ is the demagnetizing field, which depends on the boundary condition and the geometric shape and size of the sample, and is uniform in a uniformly magnetized ellipsoidal sample, but nonuniform in a rectangular body.

Referring to Bertram [53] and Schlömann [54], for uniformly magnetized bodies, the relationship between the demagnetizing field at the material point $\boldsymbol{x}$ and magnetization vector can be written as:

$$\boldsymbol{H}^{d}\left(\boldsymbol{x}\right) = \boldsymbol{D}\left(\boldsymbol{x}\right) \cdot \boldsymbol{M} \tag{8}$$

where $\boldsymbol{D}\left(\boldsymbol{x}\right)$ is the demagnetization factor, i.e.,

$$\boldsymbol{D}\left(\boldsymbol{x}\right) = -\frac{1}{4\pi} \int\!\!\int_{\partial\Omega} \frac{\boldsymbol{x} - \boldsymbol{x}'}{|\boldsymbol{x} - \boldsymbol{x}'|^{3}} \otimes \boldsymbol{n}'\mathrm{d}A' \tag{9}$$

where $\partial\Omega$ is the surface of the region occupied by the magnetized body, $\boldsymbol{x}'$ is a material point on the surface, and $\boldsymbol{n}'$ is the unit outward normal.

To accurately simulate the demagnetization effect, a magneto-mechanically coupled boundary problem should be solved after the constitutive model has been implemented into a finite element code [55]. However, in this work, only the construction of constitutive model is focused on. Thus, the heterogeneity of demagnetizing field is neglected and the demagnetization effect is considered by an average demagnetization factor $\bar{D}$, i.e.,

$$\bar{D} = -\frac{1}{4\pi V} \int \int \int_V \left(\int \int_{\partial\Omega} \frac{x - x'}{|x - x'|^3} \otimes n' \mathrm{d}A' \right) \mathrm{d}V \tag{10}$$

where V is the volume of the region occupied by the magnetized body. From Eq. (10), it is seen that $\bar{D}$ can be determined once the geometric shape of the sample is known.

So, the relationship among the internal magnetic field, external magnetic field and magnetization vector can be written as:

$$\varphi\left(H, H^{\mathrm{app}}, \sigma, T, \xi\right) = H - H^{\mathrm{app}} + \bar{D} \cdot M\left(H, \sigma, T, \xi\right) = H - H^{\mathrm{app}} + F\left(H, \sigma, T, \xi\right)\bar{D} \cdot N = 0 \tag{11}$$

where $N = H/|H|$ is the direction of magnetic field. Equation (11) can be regarded as an additional constraint on the constitutive equations.

Taking the time derivative of Eq. (11), $\dot{H}$ can be represented by $\dot{H}^{\mathrm{app}}$, $\dot{T}$ and $\dot{\xi}$, i.e.,

$$\dot{H} = -\varphi_{,H}^{-1} \cdot \varphi_{,H^{\mathrm{app}}} \cdot \dot{H}^{\mathrm{app}} - \varphi_{,H}^{-1} \cdot \varphi_{,T}\dot{T} - \varphi_{,\mathrm{H}}^{-1} \cdot \varphi_{,\sigma} : \dot{\sigma} - \varphi_{,\mathrm{H}}^{-1} \cdot \varphi_{,\xi}\dot{\xi} \tag{12}$$

where

$$\varphi_{,H} = 1 + F_{,H} \otimes \bar{D} \cdot N + F\bar{D} \cdot N_{,H} \tag{13a}$$

$$N_{,H} = \frac{\partial}{\partial H}\left(\frac{H}{|H|}\right) = \left(\frac{1 - N \otimes N}{|H|}\right) \tag{13b}$$

$$\varphi_{,H^{\mathrm{app}}} = -1 \tag{13c}$$

$$\varphi_{,T} = F_{,T}\bar{D} \cdot n \tag{13d}$$

$$\varphi_{,\xi} = F_{,\xi}\bar{D} \cdot n \tag{13e}$$

3.2. Framework of Irreversible Thermodynamics

The thermodynamic state of the material can be defined by the observable external variables and introduced internal variables. The total Gibbs free energy is decomposed into five parts, i.e.,

$$G = G_{\mathrm{mech}} + G_{\mathrm{thermal}} + G_{\mathrm{chemical}} + G_{\mathrm{Zeeman}} + G_{\mathrm{hardening}} \tag{14}$$

The mechanical energy G_{mech} consists of two parts, i.e., the energy stored by the elastic deformation and the one caused by the interaction between the stress and inelastic strain, i.e.,

$$G_{\mathrm{mech}}\left(\sigma, T, \varepsilon^{\mathrm{tr}}\right) = -\frac{1}{2\rho}\sigma : S : \sigma - \frac{1}{\rho}\sigma : \alpha\left(T - T_0\right) - \frac{1}{\rho}\sigma : \varepsilon^{\mathrm{tr}} \tag{15}$$

where ρ is the density, and S is the elastic compliance tensor. In this work, the differences of the elastic compliance tensors between austenite and martensite phases are neglected for simplicity. In this case, S is a constant tensor. For the polycrystalline aggregates, S can be regarded as a fourth-order isotropic tensor, i.e., $S = \frac{E\nu}{(1-2\nu)(1+\nu)}1 \otimes 1 + \frac{E}{1+\nu}I$, where E and ν are elastic modulus and Poisson's ratio, respectively, and I is the fourth-order unit tensor.

The thermal energy is given as follows by referring to Lagoudas et al. [49]

$$G_{\mathrm{thermal}}\left(T\right) = c\left[\left(T - T_0\right) - T\ln\left(\frac{T}{T_0}\right)\right] \tag{16}$$

where c is the specific heat at a constant volume.

Referring to Yu et al. [56], the chemical energy can be written as:

$$G_{\mathrm{chemical}}\left(T, \xi\right) = \beta\left(T - T_0\right)\xi \tag{17}$$

where β is the coefficient of entropy difference between the austenite and martensite phases.

The Zeeman energy is directly proportional to the negative value of the product of magnetization and magnetic field intensities, which can be written as

$$G_{\text{Zeeman}}(\boldsymbol{H}, T, \boldsymbol{\sigma}, \xi) = -\frac{\mu_0}{\rho} \boldsymbol{H} \cdot \boldsymbol{M} = -\frac{\mu_0}{\rho} \boldsymbol{H} \cdot \left[(1 - \xi) \boldsymbol{M}^{\text{A}} + \xi \boldsymbol{M}^{\text{M}} \right]$$
$$= -\frac{\mu_0}{\rho} \left[(1 - \xi) L^{\text{A}}(\boldsymbol{H}, T, \boldsymbol{\sigma}) + \xi L^{\text{M}}(\boldsymbol{H}, T, \boldsymbol{\sigma}) \right] \tag{18}$$

where L^{A} and L^{M} are two functions of $\boldsymbol{H}$, T and $\boldsymbol{\sigma}$, i.e., $\frac{\partial L^{\text{A}}}{\partial \boldsymbol{H}} = f(\boldsymbol{H}, T, \boldsymbol{\sigma}) \frac{\boldsymbol{H}}{|\boldsymbol{H}|}$, $\frac{\partial L^{\text{M}}}{\partial \boldsymbol{H}} = g(\boldsymbol{H}, T, \boldsymbol{\sigma}) \frac{\boldsymbol{H}}{|\boldsymbol{H}|}$, and μ_0 is the vacuum permeability.

The hardening energy reflects the transformation resistance caused by the defects (for instance, dislocation and grain boundary) in material and is a function of the volume fraction of martensite, i.e.,

$$G_{\text{hardening}}(\xi) = \frac{1}{\rho} h(\xi) \tag{19}$$

Taking the time derivative of Gibbs free energy, we obtain:

$$\dot{G} = \frac{\partial G}{\partial \boldsymbol{\sigma}} : \dot{\boldsymbol{\sigma}} + \frac{\partial G}{\partial \boldsymbol{H}} \cdot \dot{\boldsymbol{H}} + \frac{\partial G}{\partial T} \dot{T} + \frac{\partial G}{\partial \boldsymbol{\varepsilon}^{\text{tr}}} : \dot{\boldsymbol{\varepsilon}}^{\text{tr}} + \frac{\partial G}{\partial \xi} \dot{\xi} \tag{20}$$

Substituting Eq. (12) into Eq. (20), we obtain:

$$\dot{G} = \frac{\partial G}{\partial \boldsymbol{\sigma}} : \dot{\boldsymbol{\sigma}} + \frac{\partial G}{\partial \boldsymbol{H}} \cdot \left(-\boldsymbol{\varphi}_{,\boldsymbol{H}}^{-1} \cdot \boldsymbol{\varphi}_{,\boldsymbol{H}^{\text{app}}} \cdot \dot{\boldsymbol{H}}^{\text{app}} - \boldsymbol{\varphi}_{,\boldsymbol{H}}^{-1} \cdot \boldsymbol{\varphi}_{,T} \dot{T} - \boldsymbol{\varphi}_{,\boldsymbol{H}}^{-1} \cdot \boldsymbol{\varphi}_{,\boldsymbol{\sigma}} : \dot{\boldsymbol{\sigma}} - \boldsymbol{\varphi}_{,\boldsymbol{H}}^{-1} \cdot \boldsymbol{\varphi}_{,\xi} \dot{\xi} \right)$$
$$+ \frac{\partial G}{\partial T} \dot{T} + \frac{\partial G}{\partial \boldsymbol{\varepsilon}^{\text{tr}}} : \dot{\boldsymbol{\varepsilon}}^{\text{tr}} + \frac{\partial G}{\partial \xi} \dot{\xi} \tag{21}$$

For a magnetic solid, the first law of thermodynamics (i.e., conservation of energy) can be written as:

$$\rho \dot{u} = \boldsymbol{\sigma} : \dot{\boldsymbol{\varepsilon}} + \boldsymbol{H} \cdot \dot{\boldsymbol{B}} - \nabla \cdot \boldsymbol{q} \tag{22}$$

where u is the internal energy, $\boldsymbol{B}$ is the magnetic induction, and $\boldsymbol{q}$ is the heat flux. The first and second terms on the right side of Eq. (22) represent the mechanical and magnetic powers, respectively.

The relationship among magnetic field, magnetization vector and magnetic induction can be written as:

$$\boldsymbol{B} = \mu_0 (\boldsymbol{H} + \boldsymbol{M}) \tag{23}$$

The well-known second law of thermodynamics (i.e., entropy imbalance) is:

$$\rho \dot{\eta} \geq -\nabla \cdot \left(\frac{\boldsymbol{q}}{T} \right) = -\frac{\nabla \cdot \boldsymbol{q}}{T} + \frac{\nabla T \cdot \boldsymbol{q}}{T^2} \tag{24}$$

where η is the entropy.

Considering the following Legendre transformations from the internal energy u to Helmholtz free energy ψ, and from the Helmholtz free energy ψ to Gibbs free energy G, i.e.,

$$\psi = u - \eta T - \frac{\mu_0}{2\rho} \boldsymbol{H} \cdot \boldsymbol{H} \tag{25a}$$

$$G = \psi - \frac{\mu_0}{\rho} \boldsymbol{H} \cdot \boldsymbol{M} - \frac{1}{\rho} \boldsymbol{\sigma} : \boldsymbol{\varepsilon} \tag{25b}$$

By Eqs. (25a) and (25b), the relationship between $\dot{\eta}$ and $\dot{G}$ can be obtained as

$$T\dot{\eta} = -\dot{G} + \dot{u} - \eta \dot{T} - \frac{\mu_0}{\rho} \boldsymbol{H} \cdot \dot{\boldsymbol{H}} - \frac{\mu_0}{\rho} \boldsymbol{M} \cdot \dot{\boldsymbol{H}} - \frac{\mu_0}{\rho} \boldsymbol{H} \cdot \dot{\boldsymbol{M}} - \frac{1}{\rho} \boldsymbol{\varepsilon} : \dot{\boldsymbol{\sigma}} - \frac{1}{\rho} \boldsymbol{\sigma} : \dot{\boldsymbol{\varepsilon}} \tag{26}$$

Substituting Eqs. (22) and (23) into Eq. (26), the conservation of energy can be written in an equivalent form:

$$\rho T \dot{\eta} = -\boldsymbol{\varepsilon} : \dot{\boldsymbol{\sigma}} - \rho \dot{G} - \rho \eta \dot{T} - \mu_0 \boldsymbol{M} \cdot \dot{\boldsymbol{H}} - \nabla \cdot \boldsymbol{q} \tag{27}$$

Substituting Eq. (27) into Eq. (24), the entropy imbalance can be rewritten in the following equivalent form:

$$-\boldsymbol{\varepsilon} : \dot{\boldsymbol{\sigma}} - \mu_0 \boldsymbol{M} \cdot \dot{\boldsymbol{H}} - \rho \dot{G} - \rho \eta \dot{T} - \frac{\nabla T \cdot \boldsymbol{q}}{T} \geq 0 \tag{28}$$

In the following subsections, Eq. (28) will be used to derive the driving force of martensite transformation and the thermodynamic constraints on constitutive equations, while Eq. (27) will be used to obtain the internal heat production caused by the intrinsic dissipation, thermal–elastic deformation, magnetization, latent heat of phase transition and spatiotemporal evolution of temperature field.

3.3. Driving Force of Martensite Transformation and Thermodynamic Constraint

Substituting Eqs. (12) and (21) into Eq. (28), we obtain:

$$- \left(\boldsymbol{\varepsilon} + \rho \frac{\partial G}{\partial \boldsymbol{\sigma}} - \left(\mu_0 \boldsymbol{M} + \rho \frac{\partial G}{\partial \boldsymbol{H}} \right) \cdot \boldsymbol{\varphi}_{,\boldsymbol{H}}^{-1} \cdot \boldsymbol{\varphi}_{,\boldsymbol{\sigma}} \right) : \dot{\boldsymbol{\sigma}} + \left(\mu_0 \boldsymbol{M} \cdot \boldsymbol{\varphi}_{,\boldsymbol{H}}^{-1} \cdot \boldsymbol{\varphi}_{,\boldsymbol{H}^{\mathrm{app}}} + \rho \frac{\partial G}{\partial \boldsymbol{H}} \cdot \boldsymbol{\varphi}_{,\boldsymbol{H}}^{-1} \cdot \boldsymbol{\varphi}_{,\boldsymbol{H}^{\mathrm{app}}} \right) \cdot \dot{\boldsymbol{H}}^{\mathrm{app}}$$

$$- \left[\rho \eta - \left(\mu_0 \boldsymbol{M} + \rho \frac{\partial G}{\partial \boldsymbol{H}} \right) \cdot \boldsymbol{\varphi}_{,\boldsymbol{H}}^{-1} \cdot \boldsymbol{\varphi}_{,T} + \rho \frac{\partial G}{\partial T} \right] \dot{T}$$

$$+ \left[-\rho \frac{\partial G}{\partial \boldsymbol{\varepsilon}^{\mathrm{tr}}} : \dot{\boldsymbol{\varepsilon}}^{\mathrm{tr}} + \left(\mu_0 \boldsymbol{M} + \rho \frac{\partial G}{\partial \boldsymbol{H}} \right) \cdot \boldsymbol{\varphi}_{,\boldsymbol{H}}^{-1} \cdot \boldsymbol{\varphi}_{,\xi} \dot{\xi} - \rho \frac{\partial G}{\partial \xi} \dot{\xi} \right] - \frac{\nabla T \cdot \boldsymbol{q}}{T} \geq 0 \tag{29}$$

Since Eq. (29) should always be satisfied with arbitrary value of $\dot{\boldsymbol{H}}^{\mathrm{app}}$, it requires:

$$\mu_0 \boldsymbol{M} = -\rho \frac{\partial G}{\partial \boldsymbol{H}} = \mu_0 \left[(1 - \xi) \frac{\partial L^{\mathrm{A}}}{\partial \boldsymbol{H}} + \xi \frac{\partial L^{\mathrm{M}}}{\partial \boldsymbol{H}} \right] = \mu_0 F (\boldsymbol{H}, T, \boldsymbol{\sigma}, \xi) \frac{\boldsymbol{H}}{|\boldsymbol{H}|} \tag{30}$$

It should be noted that the relationship between $\boldsymbol{M}$ and $\boldsymbol{H}$ derived by thermodynamics is consistent with the previous definition [Eq. (6)].

Meanwhile, Eq. (29) should always be satisfied with arbitrary values of $\dot{\boldsymbol{\sigma}}$ and $\dot{T}$. We obtain

$$\boldsymbol{\varepsilon} = -\rho \frac{\partial G}{\partial \boldsymbol{\sigma}} + \left(\mu_0 \boldsymbol{M} + \rho \frac{\partial G}{\partial \boldsymbol{H}} \right) \cdot \boldsymbol{\varphi}_{,\boldsymbol{H}}^{-1} \cdot \boldsymbol{\varphi}_{,\boldsymbol{\sigma}} = -\rho \frac{\partial G}{\partial \boldsymbol{\sigma}} = \boldsymbol{S} : \boldsymbol{\sigma} + \boldsymbol{\alpha} (T - T_0) + \boldsymbol{\varepsilon}^{\mathrm{tr}} \tag{31a}$$

$$\rho \eta = \left(\mu_0 \boldsymbol{M} + \rho \frac{\partial G}{\partial \boldsymbol{H}} \right) \cdot \boldsymbol{\varphi}_{,\boldsymbol{H}}^{-1} \cdot \boldsymbol{\varphi}_{,T} - \rho \frac{\partial G}{\partial T} = -\rho \frac{\partial G}{\partial T}$$

$$= \boldsymbol{\sigma} : \boldsymbol{\alpha} + \rho c \ln \left(\frac{T}{T_0} \right) - \rho \beta \xi + \mu_0 \left[(1 - \xi) \frac{\partial L^{\mathrm{A}}}{\partial T} + \xi \frac{\partial L^{\mathrm{M}}}{\partial T} \right] \tag{31b}$$

Comparing Eq. (31a) with the decomposition of the total strain [Eq. (1)], it is seen that the elastic strain can be given as $\boldsymbol{\varepsilon}^{\mathrm{e}} = \boldsymbol{S} : \boldsymbol{\sigma}$, which is the well-known generalized Hooke's law.

Considering the Fourier's law of heat flux, i.e.,

$$\boldsymbol{q} = -\boldsymbol{k} \cdot \nabla T \tag{32}$$

where $\boldsymbol{k}$ is the heat conductivity coefficient, a second-order positive definite tensor, and the dissipation of heat flux in Eq. (29) is nonnegative, i.e.,

$$- \frac{\nabla T \cdot \boldsymbol{q}}{T} = \frac{\boldsymbol{k} : (\nabla T \otimes \nabla T)}{T} \tag{33}$$

Then, the intrinsic dissipation in Eq. (29) can be obtained as

$$\begin{aligned} \Gamma_{\mathrm{int}} &= -\rho \frac{\partial G}{\partial \boldsymbol{\varepsilon}^{\mathrm{tr}}} : \dot{\boldsymbol{\varepsilon}}^{\mathrm{tr}} + \left(\mu_0 \boldsymbol{M} + \rho \frac{\partial G}{\partial \boldsymbol{H}} \right) \cdot \boldsymbol{\varphi}_{,\boldsymbol{H}}^{-1} \cdot \boldsymbol{\varphi}_{,\xi} \dot{\xi} - \rho \frac{\partial G}{\partial \xi} \dot{\xi} \\ &= -\rho \frac{\partial G}{\partial \boldsymbol{\varepsilon}^{\mathrm{tr}}} : \dot{\boldsymbol{\varepsilon}}^{\mathrm{tr}} - \rho \frac{\partial G}{\partial \xi} \dot{\xi} \geq 0 \end{aligned} \tag{34}$$

Substituting Eqs. (3), (14–19) into Eq. (34), the intrinsic dissipation can be written as

$$\Gamma_{\mathrm{int}} = \left[\boldsymbol{\sigma} : \boldsymbol{\Lambda}^{\mathrm{tr}} - \rho \beta (T - T_0) + \mu_0 \left(L^{\mathrm{M}} - L^{\mathrm{A}} \right) - \frac{\partial h}{\partial \xi} \right] \dot{\xi} \geq 0 \tag{35}$$

By Eq. (35), the thermodynamic driving force of martensite transformation is defined as

$$\pi = \boldsymbol{\sigma} : \boldsymbol{\Lambda}^{\mathrm{tr}} - \rho \beta (T - T_0) + \mu_0 \left(L^{\mathrm{M}} - L^{\mathrm{A}} \right) - \frac{\partial h}{\partial \xi} \tag{36}$$

From Eq. (36), it is seen that the driving force consists of four parts, i.e., the mechanical, thermal, magnetic and transformation resistance ones.

By Eq. (35), it is seen that if no martensite transformation occurs, i.e., $\dot{\xi} = 0$, the dissipative inequality can be satisfied automatically and there is no constraint for the thermodynamic force π. If the forward transformation (from the austenite to martensite phase) occurs, i.e., $\dot{\xi} > 0$, the dissipative inequality can be satisfied when π is positive. Similarly, if the reverse transformation (from the induced martensite to austenite phase) occurs, i.e., $\dot{\xi} < 0$, the dissipative inequality can be satisfied when $\boldsymbol{\pi}$ is negative, i.e.,

$$\dot{\xi} = 0 \text{ no constraint} \tag{37a}$$

$$\dot{\xi} > 0 \quad \pi = Y \tag{37b}$$

$$\dot{\xi} < 0 \quad \pi = -Y \tag{37c}$$

where Y is a positive constant reflecting the transformation dissipation.

By Eqs. (37b) and (37c), the forward and reverse transformation surfaces are defined as

$$\Phi^{\mathrm{for}}(\boldsymbol{\sigma}, T, \boldsymbol{H}, \xi) = \pi(\boldsymbol{\sigma}, T, \boldsymbol{H}, \xi) - Y \leq 0 \tag{38a}$$

$$\Phi^{\mathrm{rev}}(\boldsymbol{\sigma}, T, \boldsymbol{H}, \xi) = -\pi(\boldsymbol{\sigma}, T, \boldsymbol{H}, \xi) - Y \leq 0 \tag{38b}$$

Then, the kinetic equations of martensite transformation can be given by the Kuhn–Tucker condition:

$$\text{Forward transformation: if } \Phi^{\mathrm{for}} = 0, \xi < 1 \text{ then } \dot{\xi}\dot{\Phi}^{\mathrm{for}} = 0 \tag{39a}$$

$$\text{Reverse transformation: if } \Phi^{\mathrm{rev}} = 0, \xi > 0 \text{ then } \dot{\xi}\dot{\Phi}^{\mathrm{rev}} = 0 \tag{39b}$$

$$\text{Elastic loading–unloading: other conditions then } \dot{\xi} = 0 \tag{39c}$$

By Eqs. (39a) and (39b), the explicit expression for the kinetic equation of forward and reverse transformation can be obtained as

$$\dot{\xi} = \frac{1}{h_{,\xi\xi}} \left\{ \begin{array}{l} \left[\boldsymbol{\Lambda}^{\mathrm{tr}} + \boldsymbol{\sigma} : \boldsymbol{\Lambda}^{\mathrm{tr}}_{,\boldsymbol{\sigma}} + \mu_0 \left(L^{\mathrm{M}} - L^{\mathrm{A}} \right)_{,\boldsymbol{\sigma}} \right] : \dot{\boldsymbol{\sigma}} - \left[\rho\beta - \boldsymbol{\sigma} : \boldsymbol{\Lambda}^{\mathrm{tr}}_{,T} - \mu_0 \left(L^{\mathrm{M}} - L^{\mathrm{A}} \right)_{,T} \right] \dot{T} \\ + \left[\boldsymbol{\sigma} : \boldsymbol{\Lambda}^{\mathrm{tr}}_{,\boldsymbol{H}} + \mu_0 \left(L^{\mathrm{M}} - L^{\mathrm{A}} \right)_{,\boldsymbol{H}} \right] \cdot \dot{\boldsymbol{H}} \end{array} \right\} \tag{40}$$

3.4. Spatiotemporal Evolution Equation of Temperature Field

Taking the time derivative of Eq. (31b), and considering the relationship between internal and external magnetic fields [Eq. (13)], we obtain

$$\rho\dot{\eta} = \dot{\boldsymbol{\sigma}} : \boldsymbol{\alpha} + \frac{\rho c \dot{T}}{T} - \rho\beta\dot{\xi} + \mu_0 \left(\frac{\partial L^{\mathrm{M}}}{\partial T} - \frac{\partial L^{\mathrm{A}}}{\partial T} + Q_1 \right) \dot{\xi}$$
$$+ \mu_0 \left[(1-\xi) \frac{\partial^2 L^{\mathrm{A}}}{\partial T^2} + \xi \frac{\partial^2 L^{\mathrm{M}}}{\partial T^2} + Q_2 \right] \dot{T} + \mu_0 \left[(1-\xi) \frac{\partial^2 L^{\mathrm{A}}}{\partial T \partial \boldsymbol{\sigma}} + \xi \frac{\partial^2 L^{\mathrm{M}}}{\partial T \partial \boldsymbol{\sigma}} + \boldsymbol{Q}_3 \right] : \dot{\boldsymbol{\sigma}} + \boldsymbol{Q}_4 \cdot \dot{\boldsymbol{H}}^{\mathrm{app}} \tag{41}$$

where

$$Q_1 = - \left[(1-\xi) \frac{\partial^2 L^{\mathrm{A}}}{\partial T \partial \boldsymbol{H}} + \xi \frac{\partial^2 L^{\mathrm{M}}}{\partial T \partial \boldsymbol{H}} \right] \cdot \boldsymbol{\varphi}_{,\boldsymbol{H}}^{-1} \cdot \boldsymbol{\varphi}_{,\xi} \tag{42a}$$

$$Q_2 = - \left[(1-\xi) \frac{\partial^2 L^{\mathrm{A}}}{\partial T \partial \boldsymbol{H}} + \xi \frac{\partial^2 L^{\mathrm{M}}}{\partial T \partial \boldsymbol{H}} \right] \cdot \boldsymbol{\varphi}_{,\boldsymbol{H}}^{-1} \cdot \boldsymbol{\varphi}_{,T} \tag{42b}$$

$$\boldsymbol{Q}_3 = - \left[(1-\xi) \frac{\partial^2 L^{\mathrm{A}}}{\partial T \partial \boldsymbol{\sigma}} + \xi \frac{\partial^2 L^{\mathrm{M}}}{\partial T \partial \boldsymbol{\sigma}} \right] \cdot \boldsymbol{\varphi}_{,\boldsymbol{H}}^{-1} \cdot \boldsymbol{\varphi}_{,\boldsymbol{\sigma}} \tag{42c}$$

$$\boldsymbol{Q}_4 = - \left[(1-\xi) \frac{\partial^2 L^{\mathrm{A}}}{\partial T \partial \boldsymbol{H}} + \xi \frac{\partial^2 L^{\mathrm{M}}}{\partial T \partial \boldsymbol{H}} \right] \cdot \boldsymbol{\varphi}_{,\boldsymbol{H}}^{-1} \cdot \boldsymbol{\varphi}_{,\boldsymbol{H}^{\mathrm{app}}} \tag{42d}$$

Substituting Eq. (41) into Eq. (27), the conservation of energy can be rewritten as

$$\rho c_{\mathrm{eff}} \dot{T} + \nabla \cdot \boldsymbol{q} = \Gamma_{\mathrm{int}} - \dot{\boldsymbol{\sigma}} : \boldsymbol{\alpha} T + T \left[\rho\beta - \mu_0 T \left(\frac{\partial L^{\mathrm{M}}}{\partial T} - \frac{\partial L^{\mathrm{A}}}{\partial T} + Q_1 \right) \right] \dot{\xi}$$
$$- \mu_0 T \boldsymbol{Q}_4 \cdot \dot{\boldsymbol{H}}^{\mathrm{app}} - \mu_0 \left[(1-\xi) \frac{\partial^2 L^{\mathrm{A}}}{\partial T \partial \boldsymbol{\sigma}} + \xi \frac{\partial^2 L^{\mathrm{M}}}{\partial T \partial \boldsymbol{\sigma}} + \boldsymbol{Q}_3 \right] : \dot{\boldsymbol{\sigma}} \tag{43}$$

where c_{eff} is the effective specific heat at a constant volume, i.e.,

$$\rho c_{\text{eff}} = \rho c + \mu_0 T \left[(1 - \xi) \frac{\partial^2 L^{\text{A}}}{\partial T^2} + \xi \frac{\partial^2 L^{\text{M}}}{\partial T^2} + Q_2 \right] \tag{44}$$

Equation (43) is the spatiotemporal evolution equation of temperature field. The first and second terms on the left side represent the variations of temperature and heat conduction, respectively, while the first, second, third and fourth terms on the right side represent the internal heat production caused by intrinsic dissipation, thermal–elastic deformation, transformation latent heat and magnetization, respectively. The fifth term is an additional heat source originated from the dependence of magnetization on the temperature and stress.

Under the adiabatic condition, the heat conduction in the material can be neglected. Then, Eq. (43) can be simplified as:

$$\rho c_{\text{eff}} \dot{T} = \Gamma_{\text{int}} - \dot{\boldsymbol{\sigma}} : \boldsymbol{\alpha} T + \rho \beta T \dot{\xi} - \mu_0 T \left(\frac{\partial L^{\text{M}}}{\partial T} - \frac{\partial L^{\text{A}}}{\partial T} + Q_1 \right) \dot{\xi}$$
$$- \mu_0 \left[(1 - \xi) \frac{\partial^2 L^{\text{A}}}{\partial T \partial \boldsymbol{\sigma}} + \xi \frac{\partial^2 L^{\text{M}}}{\partial T \partial \boldsymbol{\sigma}} + \boldsymbol{Q}_3 \right] : \dot{\boldsymbol{\sigma}} - \mu_0 T \boldsymbol{Q}_4 \cdot \dot{\boldsymbol{H}}^{\text{app}} \tag{45}$$

So far, a general constitutive framework has been established to describe the thermo-magneto-mechanically coupled deformation of MSMAs. It should be noted that the proposed constitutive equations are not limited to a specific MSMA.

4. Verification and Discussion

In this section, the proposed model is used to simulate the magnetostrictive effect of MnNiFeSn MSMA (Lázpita et al. [45]) and magnetocaloric effect of NiMnIn MSMA (Liu et al. [23]) at various temperatures, and the capability of the proposed model is verified.

4.1. Magnetostrictive Effect of MnNiFeSn MSMA

Before the prediction by the proposed model, the material parameters should be determined first. Referring to Yu et al. [56], the balance temperature T_0 can be chosen as:

$$T_0 = M_{\text{s}}^0 + \frac{Y}{\beta} \tag{46}$$

Other material parameters in the proposed model can be determined by the experimental data. The coefficient of thermal expansion can be determined from the temperature strain response, i.e., $\Delta \boldsymbol{\varepsilon} / \Delta T$, as shown in Fig. 2a. It should be noted that no mechanical load was applied in Lázpita et al. [45]. So, the term $\sqrt{\frac{3}{2}} H^{\text{max}} (\boldsymbol{\sigma}, T, \boldsymbol{H}) \frac{\text{dev}(\boldsymbol{\sigma})}{\|\text{dev}(\boldsymbol{\sigma})\|}$ in Eq. (4) keeps as zero and can be neglected. Meanwhile, $\gamma (\boldsymbol{\sigma}, T, \boldsymbol{H})$, $f (\boldsymbol{H}, T, \boldsymbol{\sigma})$ and $g (\boldsymbol{H}, T, \boldsymbol{\sigma})$ are reduced as $\gamma (T, \boldsymbol{H})$, $f (\boldsymbol{H}, T)$ and $g (\boldsymbol{H}, T)$, respectively. Moreover, the material parameters E and ν are not necessary any more.

For simplicity, the dependence of $\gamma (T, \boldsymbol{H})$ on temperature is neglected. Based on the experimental observation, $\gamma (\boldsymbol{H})$ is proposed as

$$\gamma (\boldsymbol{H}) = \gamma_\infty + (\gamma_0 - \gamma_\infty) \exp (-a_\gamma |\mu_0 \boldsymbol{H}|) \tag{47}$$

where γ_∞ and γ_0 are the volumetric strains caused by the martensite transformation under zero and a large magnetic field, respectively, and can be obtained from Fig. 2a, e.

As mentioned above, once a magnetic field is applied, the magnetizations of austenite and martensite phases in MnNiFeSn SMSA increase rapidly, but are not saturated even under a very large magnetic field. To describe this phenomenon, $f (\boldsymbol{H}, T)$ and $g (\boldsymbol{H}, T)$ are proposed as

$$f (\boldsymbol{H}, T) = M^{\text{A}} (T) [1 - \exp (-a_{\text{A}} |\mu_0 \boldsymbol{H}|)] + c_{\text{A}} |\mu_0 \boldsymbol{H}| \tag{48a}$$
$$g (\boldsymbol{H}, T) = M^{\text{M}} (T) [1 - \exp (-a_{\text{M}} |\mu_0 \boldsymbol{H}|)] + c_{\text{M}} |\mu_0 \boldsymbol{H}| \tag{48b}$$

where a_{A}, c_{A}, a_{M} and c_{M} are four material parameters; $M_{\text{A}} (T)$ and $M_{\text{M}} (T)$ reflect the dependence of magnetizations of austenite and martensite phases on temperature, respectively. From Fig. 3, it is seen that the temperature magnetization response is approximately linear when the alloy consists of pure

austenite or pure martensite phase (segments a-b and c-d). Thus, $M^A(T)$ and $M^M(T)$ are proposed as two linear functions, i.e.,

$$M^A(T) = M_0^A + b_A(T - T_0) \tag{49a}$$
$$M^M(T) = M_0^M + b_M(T - T_0) \tag{49b}$$

where M_0^A, b_A, M_0^M and b_M are four material parameters.

b_A and b_M can be obtained by fitting the experimental data of $\Delta \boldsymbol{M}^A/\Delta T$ and $\Delta \boldsymbol{M}^M/\Delta T$ from the temperature magnetization response, as shown in Fig. 3. Then, the parameters M_0^A, a_A and c_A can be determined by fitting the magnetic field magnetization response of the alloy at 230 K. Similarly, the parameters M_0^M, a_M and c_M can be determined by fitting the magnetic field magnetization response at 160 K.

By Eqs. (48a) and (48b), $L^A(\boldsymbol{H},T)$ and $L^M(\boldsymbol{H},T)$ can be obtained as

$$L^A(\boldsymbol{H},T) = M^A(T)\left[|\boldsymbol{H}| + \frac{1}{\mu_0 a_A}\exp\left(-a_A|\mu_0\boldsymbol{H}|\right)\right] + \frac{c_A}{2}\mu_0|\boldsymbol{H}|^2 \tag{50a}$$

$$L^M(\boldsymbol{H},T) = M^M(T)\left[|\boldsymbol{H}| + \frac{1}{\mu_0 a_M}\exp\left(-a_M|\mu_0\boldsymbol{H}|\right)\right] + \frac{c_M}{2}\mu_0|\boldsymbol{H}|^2 \tag{50b}$$

The transformation hardening function $h(\xi)$ is proposed as

$$h(\xi) = \frac{1}{2}C_1\xi^2 + \frac{1}{n+1}C_2\xi^{n+1} \tag{51}$$

where C_1, C_1 and n are three material parameters. The second term in Eq. (51) is introduced here to describe the nonlinear transformation hardening occurring at the end of forward transformation and the beginning of reverse transformation. C_1, C_1 and n can be obtained by fitting the linear and nonlinear hardening parts of martensite transformation in the temperature strain response, respectively, as shown in Fig. 2a.

In Fig. 2e, M_s^{12} denotes the start temperature of martensite transformation under an applied magnetic field of 12 T. However, owing to the demagnetization effect, the internal magnetic field is not always equal to the applied magnetic field. Recalling Eqs. (6) and (11), the relationship between $\boldsymbol{H}_{M_s^{12}}$ (the internal magnetic field at M_s^{12}) and $\boldsymbol{H}^{\text{app}}$ can be written as (noted that at this point, $\xi=0$):

$$\boldsymbol{H}_{M_s^{12}} = \boldsymbol{H}^{\text{app}} - f\left(\boldsymbol{H}_{M_s^{12}}, M_s^{12}\right)\bar{\boldsymbol{D}}\cdot\frac{\boldsymbol{H}_{M_s^{12}}}{\left|\boldsymbol{H}_{M_s^{12}}\right|} \text{ at } M_s^{12} \tag{52}$$

Then, $\boldsymbol{H}_{M_s^{12}}$ can be solved by Eq. (52). Considering Eqs. (36), (38a) and the relationship between T_0 and M_s^0, the following transformation condition should be satisfied at M_s^{12}, i.e.,

$$\Phi^{\text{for}}\left(\boldsymbol{0}, M_s^{12}, \boldsymbol{H}_{M_s^{12}}, 0\right) = -\rho\beta\left(M_s^{12} - M_s^0\right) + \mu_0\left[L^M\left(\boldsymbol{H}_{M_s^{12}}, M_s^{12}\right) - L^A\left(\boldsymbol{H}_{M_s^{12}}, M_s^{12}\right)\right] = 0 \tag{53}$$

Then, the parameter β can be obtained by Eq. (53).

Without an applied magnetic field, the following transformation conditions should be satisfied at M_f^0 and A_s^0 (noted that at these two points, $\xi=1$)

$$\Phi^{\text{for}}\left(\boldsymbol{0}, M_f^0, \boldsymbol{0}, 1\right) = -\rho\beta\left(M_f^0 - M_s^0\right) - C_1 - C_2 = 0 \tag{54a}$$
$$\Phi^{\text{rev}}\left(\boldsymbol{0}, A_s^0, \boldsymbol{0}, 1\right) = -\rho\beta\left(A_s^0 - M_s^0\right) - C_1 - C_2 + 2Y = 0 \tag{54b}$$

By Eqs. (54a) and (54b), the material parameter Y can be obtained.

It should be noted that in Lázpita et al. [45], the loading rate is very small, which can be regarded as a quasi-static one. So, the effect of internal heat production on deformation and magnetization can be neglected. Thus, in this subsection, the temperature of the sample is assumed to be identical to the ambient temperature.

Using the material parameters listed in Table 1, the proposed model is used to simulate the above-mentioned experimental results, as shown in Figs. 1, 2, 3 and 4. It should be noted that the agreements between the experimental and simulated results shown in Figs. 1, 2a, e and 3 are expected, because the material parameters used in the proposed model are calibrated from the experimental data shown in

Table 1. **Material parameters used in the proposed model for simulating the temperature-induced martensite transformation and magnetostrictive effect in MnNiFeSn MSMA**

$\rho = 8000 \, \text{kg/m}^3; \alpha = 12 \times 10^{-6}/\text{K};$
$a_\text{A} = 10/T; c_\text{A} = 1.26 \times 10^4 \, \text{A/(Tm)}; M_0^\text{A} = 3.7 \times 10^5 \, \text{A/m}; b_\text{A} = -2.5 \times 10^3 \, \text{A/(Km)};$
$a_\text{M} = 10/T; c_\text{M} = 6.67 \times 10^3 \, \text{A/(Tm)}; M_0^\text{M} = 8.0 \times 10^4 \, \text{A/m}; b_\text{M} = -3.0 \times 10^2 \, \text{A/(Km)};$
$\rho\beta = 0.2 \, \text{MPa/K}; Y = 0.85 \, \text{MPa}; C_1 = 2 \, \text{MPa}; C_2 = 0.55 \, \text{MPa}; n = 10;$
$\gamma_0 = 4.3 \times 10^{-3}; \gamma_\infty = 3.6 \times 10^{-3}; a_\gamma = 10/T.$

these figures. However, comparing the predicted results (Figs. 2b–d, 4a, b) with the experimental ones (which are not used in the calibration of material parameters), it is concluded that the temperature-induced martensite transformation with various applied magnetic fields and the magnetostrictive effect at different temperatures for the MnNiFeSn MSMA can be quantitatively described by the proposed model. Surely, there are some discrepancies between the experimental and simulated hysteresis loops in the magnetic field strain responses, as shown in Fig. 4. In fact, the material parameters related to the transformation hardening are fitted from the temperature strain response (as shown in Fig. 2a). Maybe the transformation hardening induced by temperature is different from that induced by magnetic field. Thus, in order to describe it more accurately, a new hardening rule which can distinguish these two processes is needed, which will be done in our future work.

It should be noted that the specific forms of the functions $\gamma\,(\boldsymbol{\sigma}, T, \boldsymbol{H})$, $f\,(\boldsymbol{H}, T, \boldsymbol{\sigma})$, $g\,(\boldsymbol{H}, T, \boldsymbol{\sigma})$ and $h\,(\xi)$ provided in this subsection only apply to the MnNiFeSn MSMA since they are determined from the experimental data of such an MSMA.

4.2. Magnetocaloric Effect of NiMnInCo MSMA

It should be noted that the deviatoric stress was not applied in Liu et al. [23]. Thus, the term $\sqrt{\frac{3}{2}} H^\text{max}\,(\boldsymbol{\sigma}, T, \boldsymbol{H})\, \frac{\text{dev}(\boldsymbol{\sigma})}{\|\text{dev}(\boldsymbol{\sigma})\|}$ in Eq. (4) is also neglected in this subsection. Moreover, due to the lack of experimental data, the dependences of γ, f and g on stress are not considered here.

The elastic modulus E and Poisson's ratio ν of the alloy are required since the influence of hydrostatic pressure on the magnetocaloric effect will be predicted and discussed by the proposed model, and are set as 12 GPa and 0.3, respectively, by referring to Haldar et al. [44] and Lagoudas et al. [49]. As reported by Liu et al. [23], the martensite phase of NiMnInCo MSMA is a nonmagnetic phase. Thus, in this subsection, $g\,(\boldsymbol{H}, T)$ is set as zero. Because the magnetic field magnetization response of austenite phase was not provided in Liu et al. [23], $f\,(\boldsymbol{H}, T)$ cannot be obtained directly. As discussed by Haldar et al. [44], the magnetization of austenite phase in NiMnInCo MSMA can be saturated even at a very low magnetic field. Then, they proposed a magnetization rule for the austenite phase in NiMnInCo MSMA as $\boldsymbol{M}^\text{A} = M_\text{sat}^\text{A} \frac{\boldsymbol{H}}{|\boldsymbol{H}|}$, where M_sat^A is the saturated magnetization of austenite phase. Referring to Haldar et al. [44] and considering the dependence of M_sat^A on temperature, $f\,(\boldsymbol{H}, T)$ can be given as:

$$f\,(\boldsymbol{H}, T) = M_\text{sat}^\text{A} + b_\text{A}\,(T - T_0) \tag{55}$$

where b_A is a material parameter and M_sat^A is the saturated magnetization of austenite phase at T_0. The two parameters can be easily obtained from the temperature magnetization response. By Eq. (55), $L^\text{A}\,(\boldsymbol{H}, T)$ can be obtained as

$$L^\text{A}\,(\boldsymbol{H}, T) = \left[M_\text{sat}^\text{A} + b_\text{A}\,(T - T_0) \right] |\boldsymbol{H}| \tag{56}$$

From Fig. 5, it is seen that the nonlinearity of temperature magnetization response is not strong during the martensite transformation. Thus, for simplicity, the nonlinear transformation hardening is neglected here, so that $h\,(\xi) = \frac{1}{2} C_1 \xi^2$. Similar to that discussed in Section 4.1, the specific forms of functions $\gamma\,(\boldsymbol{\sigma}, T, \boldsymbol{H})$, $f\,(\boldsymbol{H}, T, \boldsymbol{\sigma})$, $g\,(\boldsymbol{H}, T, \boldsymbol{\sigma})$ and $h\,(\xi)$ proposed here only apply to the NiMnInCo MSMA since they are determined from the experimental data of such an MSMA.

As mentioned above, the internal magnetic field is not always equal to the applied magnetic field due to the demagnetization effect. Recalling Eqs. (6) and (11), the relationship between $\boldsymbol{H}$ and $\boldsymbol{H}^\text{app}$ at $M_\text{s}^{0.01}$, M_s^2 (noted that at these two points, $\xi=0$), M_f^2 and A_s^2 (noted that at these two points, $\xi=1$)

Table 2. **Material parameters used in the proposed model for simulating the magnetocaloric effect in NiMnInCo MSMA**

$\rho = 8020$ kg/m^3; $\alpha = 12 \times 10^{-6}$/K; $\rho c = 3.2$ MJ/(m^{3}K)
$M_0^A = 3.38 \times 10^5$ A/m; $b_A = -2.6 \times 10^3$ A/Km;
$\rho\beta = 0.14$ MPa/K; $Y = 0.53$ MPa; $C_1 = 1.2$ MPa;
$E = 12$ GPa; $v = 0.3$; $\gamma_0 = 4.3 \times 10^{-3}$; $\gamma_\infty = 3.6 \times 10^{-3}$; $a_\gamma = 10$/T.

can be written as:

$$\boldsymbol{H}_{M_s^{0.01}} = \boldsymbol{H}^{\text{app}} - f\left(\boldsymbol{H}_{M_s^{0.01}}, M_s^{0.01}\right) \bar{\boldsymbol{D}} \cdot \frac{\boldsymbol{H}_{M_s^{0.01}}}{\left|\boldsymbol{H}_{M_s^{0.01}}\right|} \text{ at } M_s^{0.01} \tag{57a}$$

$$\boldsymbol{H}_{M_s^2} = \boldsymbol{H}^{\text{app}} - f\left(\boldsymbol{H}_{M_s^2}, M_s^2\right) \bar{\boldsymbol{D}} \cdot \frac{\boldsymbol{H}_{M_s^2}}{\left|\boldsymbol{H}_{M_s^2}\right|} \text{ at } M_s^2 \tag{57b}$$

$$\boldsymbol{H}_{M_f^2} = \boldsymbol{H}_{A_s^2} = \boldsymbol{H}^{\text{app}} \text{ at } M_f^2 \text{ and } A_s^2 \tag{57c}$$

Then, $\boldsymbol{H}_{M_s^{0.01}}$, $\boldsymbol{H}_{M_s^2}$, $\boldsymbol{H}_{M_f^2}$ and $\boldsymbol{H}_{A_s^2}$ can be solved by Eqs. (57a), (57b) and (57c).

Considering Eqs. (36), (38a) and the relationship between T_0 and M_s^0, the following transformation conditions should be satisfied at $M_s^{0.01}$, M_s^2, M_f^2 and A_s^2, i.e.,

$$\Phi^{\text{for}}\left(\boldsymbol{0}, M_s^{0.01}, \boldsymbol{H}_{M_s^{0.01}}, 0\right) = -\rho\beta\left(M_s^{0.01} - M_s^0\right) - \mu_0 L^A\left(\boldsymbol{H}'_{M_s^{0.01}} M_s^{0.01}\right) = 0 \tag{58a}$$

$$\Phi^{\text{for}}\left(\boldsymbol{0}, M_s^2, \boldsymbol{H}_{M_s^2}, 0\right) = -\rho\beta\left(M_s^2 - M_s^0\right) - \mu_0 L^A\left(\boldsymbol{H}'_{M_s^2} M_s^2\right) = 0 \tag{58b}$$

$$\Phi^{\text{for}}\left(\boldsymbol{0}, M_f^2, \boldsymbol{H}_{M_f^2}, 1\right) = -\rho\beta\left(M_f^2 - M_s^0\right) - \mu_0 L^A\left(\boldsymbol{H}'_{M_f^2} M_f^2\right) - C_1 = 0 \tag{58c}$$

$$\Phi^{\text{rev}}\left(\boldsymbol{0}, A_s^2, \boldsymbol{H}_{A_s^2}, 1\right) = -\rho\beta\left(A_s^2 - M_s^0\right) - \mu_0 L^A\left(\boldsymbol{H}'_{A_s^2} A_s^2\right) - C_1 + 2Y = 0 \tag{58d}$$

By Eqs. (54a), (54b) and (55), M_s^0, β, Y and C_1 can be obtained.

However, γ and α cannot be determined since the volumetric strain caused by the martensite transformation and the thermal expansion strain were not measured in Liu et al. [23]. Thus, in this subsection, γ and α are kept the same as those in Section 3.1.

Using the material parameters listed in Table 2, the proposed model is used to simulate the experimental results shown in Figs. 5, 6 and 7. It should be noted that all the material parameters are calibrated only from the experimental data shown in Fig. 5, and the magnetocaloric effect (as shown in Figs. 6 and 7) is predicted by the proposed model. Comparing the predicted results with the experimental ones, it is seen that the magnetocaloric effect of NiMnInCo MSMA can be reasonably described, since the internal heat production caused by the intrinsic dissipation, thermo-elastic deformation, magnetization and the latent heat of phase transition have been considered in the proposed model. It should be pointed out that four material parameters E, ν, γ and α are not determined by the experimental results from Liu et al. [23] but by referring to [44, 49]. However, the simulated results shown in Figs. 5, 6 and 7 do not depend on these four material parameters.

As mentioned above, the main drawbacks of magnetic refrigeration are the narrow range of working temperature and the unrecoverable temperature change after the applied magnetic field is removed. To better illustrate these problems, the temperature evolutions under a cyclic loading of magnetic field with 10 cycles and at various ambient temperatures are predicted by the proposed model. In each cycle, the loading path is kept the same as that in Liu et al. [23], i.e., 0 T → 2 T → 0 T → −2 T → 0 T. Figure 8a shows the predicted results. It is seen from Fig. 8a that at 302 K, no temperature oscillation can be observed since the martensite phase is a nonmagnetic phase. At 310 K and 317 K, obvious temperature oscillation is observed and the amplitudes are 2.2 K and 1.8 K, respectively. The temperature oscillation at these two temperatures is mainly originated from the release/absorption of latent heat during the MFIT and its reverse. Meanwhile, it can be seen that the average temperature (the mean value of the maximum and minimum temperatures in each loading cycle) increases with the increasing number of cycles, which is caused by the accumulated intrinsic dissipation [57, 58]. However, at 325 K and 334 K, the temperature oscillation becomes very small again. In fact, at these two temperatures, the alloy

consists of pure austenite phase, and the reverse transformation cannot be induced by the magnetic field. Thus, the temperature oscillation is only originated from the internal heat production caused by the magnetization [i.e., the fourth term on the right side of Eq. (43)].

The narrow range of working temperature and the unrecoverable temperature change hinders the wide application of MSMAs. Fortunately, a large inelastic strain produced by the martensite transformation provides an effective pathway to improve the magnetocaloric effect of MSMAs by stress manipulation (i.e., by applying an additional and suitable stress). In this subsection, as per the prediction by the proposed model, some magneto-mechanically coupled loading paths are designed to improve the magnetocaloric effect of NiMnInCo MSMA.

The magneto-mechanically coupled loading paths in each cycle are given in Fig. 8b at the ambient temperatures of 302 K, 310 K, 317 K, 325 K and 334 K. The loading path of magnetic field is kept unchanged, but an additional hydrostatic pressure is applied, simultaneously. Then, the temperature evolutions of the alloy at various ambient temperatures are predicted by the proposed model, and the results are shown in Fig. 8c. Comparing Fig. 8c with Fig. 8a, it is seen that a large temperature oscillation ($> 6\mathrm{K}$) occurs in the cases with an additional hydrostatic pressure and at each ambient temperature. In fact, since the driving force of martensite transformation contains a mechanical part [as shown in Eq. (36)], the applied stress can change the evolution rate of the volume fraction of martensite phase during the MFIT and further the amount of internal heat production. Therefore, the magnetocaloric effect can be significantly improved by an additional applied stress.

It should be noted that other forms of stresses, for instance, the axial stress, biaxial stress and shear stress, can also be adopted to manipulate the magnetocaloric effect of MSMAs. In these cases, the term $\sqrt{\frac{3}{2}} H^{\mathrm{max}}\left(\boldsymbol{\sigma}, T, \boldsymbol{H}\right) \frac{\mathrm{dev}(\boldsymbol{\sigma})}{\|\mathrm{dev}(\boldsymbol{\sigma})\|}$ in Eq. (4) cannot be neglected any more. However, due to the lack of experimental data, the function $H^{\mathrm{max}}\left(\boldsymbol{\sigma}, T, \boldsymbol{H}\right)$ cannot be determined in this work. Thus, only the hydrostatic pressure is discussed here.

5. Conclusion

1. A macroscopic phenomenological constitutive model is established for modeling the thermo-magneto-mechanically coupled deformation of polycrystalline MSMAs. The thermodynamic driving force of martensite transformation, internal heat production during the deformation and magnetization and the constraints on the constitutive equations are deduced by the dissipative inequality and introduced Gibbs free energy. The spatiotemporal evolution equation of temperature field is deduced by the first law of thermodynamics. Meanwhile, the demagnetization effect in the magnetization process is addressed.
2. Comparing the predicted results with the corresponding experimental ones, it is seen that the thermo-magneto-mechanically coupled deformation of polycrystalline MSMAs, including the magnetostrictive and magnetocaloric effects, can be reasonably described by the proposed model.
3. Some magneto-mechanically coupled loading paths are designed and proved to manipulate the magnetocaloric effect of MSMAs so that the main drawbacks of magnetic refrigeration, i.e., the narrow range of working temperature and the unrecoverable temperature change after the applied magnetic field is removed, can be improved. The predicted results given by the proposed model show that the magnetocaloric effect can be significantly improved by introducing an additional applied stress, which provides an effective pathway for designing the magnetic refrigerator made by MSMAs.

References

[1] Sarawate N, Dapino M. Experimental characterization of the sensor effect in ferromagnetic shape memory NiMnGa. Appl Phys Lett. 2006;88:121923.
[2] Sarawate N, Dapino M. A continuum thermodynamics model for the sensing effect in ferromagnetic shape memory Ni–Mn–Ga. J Appl Phys. 2007;101:123522.

[3] Karaman I, Basaran B, Karaca HE, Karsilayan AI, Chumlyakov YI. Energy harvesting using martensite variant reorientation mechanism in a NiMnGa magnetic shape memory alloy. Appl Phys Lett. 2007;90(17):172505.

[4] Qu YH, Cong DY, Li SH, Gui WY, Nie ZH, Zhang MH, Ren Y, Wang YD. Simultaneously achieved large reversible elastocaloric and magnetocaloric effects and their coupling in a magnetic shape memory alloy. Acta Mater. 2017;151:41–55.

[5] Ullakko K, Huang JK, Kantner C, O'handley RC, Kokorin VV. Large magnetic-field-induced strains in Ni2MnGa single crystals. Appl Phys Lett. 1996;69(13):1966–8.

[6] Murray SJ, Marioni M, Allen SM, O'handley RC, Lograsso TA. 6% magnetic-field-induced strain by twin-boundary motion in ferromagnetic Ni–Mn–Ga. Appl Phys Lett. 2000;77(6):886–8.

[7] Karaca HE, Karaman I, Basaran B, Chumlyakov YI, Maier HJ. Magnetic field and stress induced martensite reorientation in NiMnGa ferromagnetic shape memory alloy single crystals. Acta Mater. 2006;54:233–45.

[8] Tickle R, James RD. Magnetic and magnetomechanical properties of Ni2MnGa. J Magn Magn Mater. 1999;195:627–38.

[9] Heczko O. Magnetic shape memory effect and magnetization reversal. J Magn Magn Mater. 2005;290:787–94.

[10] Straka L, Heczko O. Reversible 6% strain of Ni–Mn–Ga martensite using opposing external stress in static and variable magnetic fields. J Magn Magn Mater. 2005;290:829–31.

[11] Cui J, Shield TW, James RD. Phase transformation and magnetic anisotropy of an iron-palladium ferromagnetic shape-memory alloy. Acta Mater. 2004;52(1):35–47.

[12] Fujita A, Fukamichi K, Gejima F, Kainuma R, Ishida K. Magnetic properties and large magnetic-field-induced strains in off-stoichiometric Ni–Mn–Al Heusler alloys. Appl Phys Lett. 2000;77(19):3054–6.

[13] Kakeshita T, Takeuchi T, Fukuda T, Tsujiguchi M, Saburi T, Oshima R, Muto S. Giant magnetostriction in an ordered Fe3Pt single crystal exhibiting a martensitic transformation. Appl Phys Lett. 2000;77(10):1502–4.

[14] Wuttig M, Li J, Craciunescu C. A new ferromagnetic shape memory alloy system. Scripta Mater. 2001;44(10):2393–7.

[15] Karaca HE, Karaman I, Lagoudas DC, Maier HJ, Chumlyakov YI. Recoverable stress-induced martensitic transformation in a ferromagnetic CoNiAl alloy. Scripta Mater. 2003;49(9):831–6.

[16] Karaca HE, Karaman I, Basaran B, Ren Y, Chumlyakov YI, Maier HJ. Magnetic field-induced phase transformation in NiMnCoIn magnetic shape-memory alloys—a new actuation mechanism with large work output. Adv Funct Mater. 2009;19(7):983–98.

[17] Liu J, Wang J, Zhang H, Jiang C, Xu H. Effect of directional solidification rate on the solidified morphologies and phase transformations of $Ni_{50.5}Mn_{25}Ga_{24.5}$ alloy. J Alloys Compd. 2012;541:477–82.

[18] Gaitzsch U, Romberg J, Pötschke M, Roth S, Müllner P. Stable magnetic-field-induced strain above 1% in polycrystalline Ni–Mn–Ga. Scripta Mater. 2011;65(8):679–82.

[19] Zhu Y, Chen T, Teng Y, Liu B, Xue L. Experimental study of directionally solidified ferromagnetic shape memory alloy under multi-field coupling. J Magn Magn Mater. 2016;417:249–57.

[20] Sutou Y, Imano Y, Koeda N, Omori T, Kainuma R, Ishida K, Oikawa K. Magnetic and martensitic transformations of NiMnX (X = In, Sn, Sb) ferromagnetic shape memory alloys. Appl Phys Lett. 2004;85(19):4358–60.

[21] Kainuma R, Imano Y, Ito W, Sutou Y, Morito H, Okamoto S, Kitakami O, Fujita A, Kanomata T, Ishida K. Magnetic-field-induced shape recovery by reverse phase transformation. Nature. 2006;439(7079):957.

[22] Kainuma R, Imano Y, Ito W, Morito H, Sutou Y, Oikawa K, Fujita A, Ishida K. Metamagnetic shape memory effect in a Heusler-type $Ni_{43}Co_7Mn_{39}Sn_{11}$ polycrystalline alloy. Appl Phys Lett. 2006;88(19):192513.

[23] Liu J, Gottschall T, Skokov KP, Moore JD, Gutfleisch O. Giant magnetocaloric effect driven by structural transitions. Nature Mater. 2012;11(7):620.

[24] Cong DY, Huang L, Hardy V, Bourgault D, Sun XM, Nie ZH, Wang MG, Ren Y, Entel P, Wang YD. Low-field-actuated giant magnetocaloric effect and excellent mechanical properties in a NiMn-based multiferroic alloy. Acta Mater. 2018;146:142–51.

[25] Qu YH, Cong DY, Sun XM, Nie ZH, Gui WY, Li RG, Ren Y, Wang YD. Giant and reversible room-temperature magnetocaloric effect in Ti-doped Ni–Co–Mn–Sn magnetic shape memory alloys. Acta Mater. 2017;134:236–48.

[26] Planes A, Mañosa L, Acet M. Magnetocaloric effect and its relation to shape-memory properties in ferromagnetic Heusler alloys. J Phys-Condens Matter. 2009;21(23):233201.

[27] Krenke T, Duman E, Acet M, Wassermann EF, Moya X, Mañosa L, Planes A. Inverse magnetocaloric effect in ferromagnetic Ni–Mn–Sn alloys. Nature Mater. 2005;4(6):450.

[28] Phan MH, Yu SC. Review of the magnetocaloric effect in manganite materials. J Magn Magn Mater. 2007;308(2):325–40.

[29] Hirsinger L, Lexcellent C. Modelling detwinning of martensite platelets under magnetic and (or) stress actions on Ni–Mn–Ga alloys. J Magn Magn Mater. 2003;254:275–7.

[30] Hirsinger L, Lexcellent C. Internal variable model for magneto-mechanical behaviour of ferromagnetic shape memory alloys Ni–Mn–Ga. J Phys IV Fr. 2003;112:977–80.

[31] Kiefer B, Lagoudas DC. Magnetic field-induced martensitic variant reorientation in magnetic shape memory alloys. Philos Mag. 2005;85:4289–329.

[32] Wang X, Li F. A kinetics model for martensite variants rearrangement in ferromagnetic shape memory alloys. J Appl Phys. 2010;108(11):113921.

[33] Couch RN, Chopra I. A quasi-static model for NiMnGa magnetic shape memory alloy. Smart Mater Struct. 2007;16(1):S11.

[34] Zhu Y, Dui G. Micromechanical modeling of the stress-induced superelastic strain in magnetic shape memory alloy. Mech Mater. 2007;39:1025–34.

[35] Zhu Y, Dui G. Model for field-induced reorientation strain in magnetic shape memory alloy with tensile and compressive loads. J Alloys Compd. 2008;459:55–60.

[36] Zhu Y, Yu K. A model considering mechanical anisotropy of magnetic-field-induced superelastic strain in magnetic shape memory alloys. J Alloys Compd. 2013;550:308–13.

[37] Wang X, Li F, Hu Q. An anisotropic micromechanical-based model for characterizing the magneto-mechanical behavior of NiMnGa alloys. Smart Mater Struct. 2012;21:065021.

[38] Chen X, Moumni Z, He Y, Zhang W. A three-dimensional model of magneto-mechanical behaviors of martensite reorientation in ferromagnetic shape memory alloys. J Mech Phys Solids. 2014;64:249–86.

[39] Auricchio F, Bessoud AL, Reali A, Stefanelli U. A phenomenological model for the magneto-mechanical response of single-crystal magnetic shape memory alloys. Eur J Mech A-Solid. 2015;52:1–11.

[40] Mousavi MR, Arghavani J. A three-dimensional constitutive model for magnetic shape memory alloys under magneto-mechanical loadings. Smart Mater Struct. 2017;26:015014.

[41] Pei Y, Fang D. A model for giant magnetostrain and magnetization in the martensitic phase of NiMnGa alloys. Smart Mater Struct. 2007;16(3):779.

[42] LaMaster DH, Feigenbaum HP, Nelson ID, Ciocanel C. A full two-dimensional thermodynamic-based model for magnetic shape memory alloys. J Appl Mech. 2014;81:061003.

[43] LaMaster DH, Feigenbaum HP, Ciocanel C, Nelson ID. A full 3D thermodynamic-based model for magnetic shape memory alloys. J Intell Mater Syst Struct. 2015;26:663–79.

[44] Haldar K, Lagoudas DC. Karaman I. Magnetic field-induced martensitic phase transformation in magnetic shape memory alloys: modeling and experiments. J Mech Phys Solids. 2014;69:33–66.

[45] Lázpita P, Sasmaz M, Barandiarán JM, Chernenko VA. Effect of Fe doping and magnetic field on martensitic transformation of Mn–Ni (Fe)–Sn metamagnetic shape memory alloys. Acta Mater. 2018;155:95–103.

[46] Mañosa L, Moya X, Planes A, Gutfleisch O, Lyubina J, Barrio M, Tamarit L, Aksoy S, Krenke T, Acet M. Effects of hydrostatic pressure on the magnetism and martensitic transition of Ni–Mn–In magnetic superelastic alloys. Appl Phys Lett. 2008;92(1):012515.

[47] Muthu SE, Rao NVR, Raja MM, Arumugam S, Matsubayasi K, Uwatoko Y. Hydrostatic pressure effect on the martensitic transition, magnetic, and magnetocaloric properties in $Ni_{50-x}Mn_{37+x}Sn_{13}$ Heusler alloys. J Appl Phys. 2011;110(8):083902.

[48] Qidwai MA, Lagoudas DC. On thermomechanics and transformation surfaces of polycrystalline NiTi shape memory alloy material. Int J Plast. 2000;16(10–11):1309–43.

[49] Lagoudas D, Hartl D, Chemisky Y, Machado L, Popov P. Constitutive model for the numerical analysis of phase transformation in polycrystalline shape memory alloys. Int J Plast. 2012;32:155–83.

[50] Anand L, Gurtin ME. Thermal effects in the superelasticity of crystalline shape-memory materials. J Mech Phys Solids. 2003;51(6):1015–58.

[51] Otsuka K, Ren X. Physical metallurgy of Ti-Ni-based shape memory alloys. Prog Mater Sci. 2005;50(5):511–678.

[52] Krenke T, Duman E, Acet M, Wassermann EF, Moya X, Mañosa L, Planes A, Suard E, Ouladdiaf B. Magnetic superelasticity and inverse magnetocaloric effect in Ni–Mn–In. Phys Rev B. 2007;75(10):104414.

[53] Bertram HN. Theory of magnetic recording. Cambridge: Cambridge University Press; 1994.

[54] Schlömann E. A sum rule concerning the inhomogeneous demagnetizing field in nonellipsoidal samples. J Appl Phys. 1962;33(9):2825–6.

[55] Haldar K, Kiefer B, Lagoudas DC. Finite element analysis of the demagnetization effect and stress inhomogeneities in magnetic shape memory alloy samples. Philos Mag. 2011;91(32):4126–57.

[56] Yu C, Kang G, Kan Q. A physical mechanism based constitutive model for temperature-dependent transformation ratchetting of NiTi shape memory alloy: one-dimensional model. Mech Mater. 2014;78:1–10.

[57] He YJ, Sun QP. Frequency-dependent temperature evolution in NiTi shape memory alloy under cyclic loading. Smart Mater Struct. 2010;19(11):115014.

[58] Yu C, Kang G, Kan Q, Zhu Y. Rate-dependent cyclic deformation of super-elastic NiTi shape memory alloy: thermo-mechanical coupled and physical mechanism-based constitutive model. Int J Plast. 2015;72:60–90.